CHAPTER 4

INITIAL INVESTIGATION ON THE PRECIPITATE SAMPLE FOR THE ADSORPTION OF CETYLTRIMETHYLAMMONIUM BROMIDE (CTAB) ONTO CALCIUM CARBONATE NANO-CUBE PARTICLES UNDER ALKALINE –AQUEOUS SOLUTION

CHAPTER 4

INITIAL INVESTIFATION ON THE PRECIPITATE SAMPLE FOR THE ADSORPTION OF CETYLTRIMETHYLAMMONIUM BROMIDE ONTO CALCIUM CARBONATE NANO-CUBE PARTICLES UNDER ALKALINE-AQUEOUS SOLUTION

4.1 Introduction

Surfactant adsorption onto inorganic nanoparticles has been important in variety of fields such as adhesion, lubrication, corrosion inhibition and detergency.[1, 2] Wherein, various types of nanoparticles are currently commercially available, e.g., silica, calcium carbonate, and carbon black, without any surface treatment are not surface active due to either their extreme hydrophilicity or hydrophobicity [3]. A popular route to obtain surface active/modified surface nanoparticles is to coat them homogeneously with synthetic surfactant. These synthetic surfactants are classified into four major types according to their head groups: anionic, cationic, nonionic and amphoteric [1, 2, 4]. In this research work, a calcium carbonate ($CaCO_3$) inorganic nanoparticle is used. It is noted that $CaCO_3$ nanoparticles represent the highest output and probably the lowest cost of commercial nanoparticles. As mention above, $CaCO_3$ nanoparticles without any surface treatment are not surface active but are edible. They are strongly hydrophilic and charged that prefer to remain dispersed in water/ethanol solution [5-7]. Technically, industrially significant if it can be made surface active or modified surface via simple methods. This is one of the important industrial minerals used in both natural and synthetic forms in the rubber, plastic and paper industries.[1, 8]

Hence, surface properties play any important role in determining the effectiveness of $CaCO_3$ as bulk filler or as functional component in a final product. As pigment in the coating of paper and board, the nature and surface morphology of $CaCO_3$ are a major factors in determining the significant properties of the final product, such as dusting, ink interaction and de-inking of waste paper[8, 9]. Wherein, physic- and chemisorbed water bound within the pore structure significantly influences the properties of $CaCO_3$.

Theoretically, when a solid is brought in contact with aqueous solution of a surface-active agent surfactant molecules adsorbed at the solid-liquid interface [1, 10, 11]. In absence of special directive force, the ions adsorbed at the interface will be oriented (as a whole) majority of their hydrophilic groups occurs towards the aqueous phase so wetting occurs. (Adsorption is non-specific). But, at initial stages of adsorption on polar solids may occur due to chemical or electrostatic interaction between the polar head groups of the surfactant and the polar solid surfaces, in most cases the head groups of the surfactant anchored to oppositely charged surfaces sites and the hydrocarbons chains directed outermost[5, 12]. The surface is rendered as hydrophobic. The contact angle becomes finite and floatation is achievable. In case of reversed orientation, a second layer of surfactant may build up at higher concentration on top of the first layer through chain-chain cohesion.[13, 14] Under this condition, rewetting occurs and contact angkle decrease and may vanish. Such adsorption phenomena are fundamental importance in technical applications such as detergency, flotation, water-proofing and etc. [5, 6, 15]

Recently, Cui et al, investigate the in situ surface activation of $CaCO_3$ nanoparticles by interaction with anionic surfactant and found out were excellent emulsion stabilizer [16, 17]. But when CTAB (cationic surfactant)–$CaCO_3$ nanoparticles mixed, no obvious synergistic effect on foaming was observed, suggested that $CaCO_3$ nanoparticles cannot be surface activated via interaction with cationic or nonionic surfactant in aqueous solution.[16]. While Shi et al., explored the chemisorbed strearate (stearic acid) on the $CaCO_3$ surface and proposed a micelle adsorption mechanism (discussed formation of monolayer's adsorp on $CaCO_3$. [18].

Ivanova et. al., reported that in accordance with the adsorption model of cationic surfactant on a charged solid surfaces; their results showed that at low (cationic dode-cylamine hydrochloride, DDAHC) surfactant concentrations (with respect to CMC), the surfactant ions are individually adsorbed onto the solid surface mainly by electrostatic attraction.[14, 19] The adsorption layer is very sparse and the surface occupied one molecule is roughly around 280 $Å^2$. On increasing the surfactant concentration, the slope of the adsorption isotherm exhibits a sharp increase. The adsorption is also accompanied by a decrease in the electrokinetic potential and a reversal of the zeta potential is observed in the same region, wherein the density of adsorption sharply increases. These facts have been attributed to the formations of aggregates (admicelles) at the calcium carbonates surfaces or adsorption of dimers [1, 14, 19] Thus, at the solid/solution interface at low concentration of cationic DDAHC, individual ions of the surfactant are adsorbed and at higher concentration (above half the CMC) aggregates of cationic $DDAH^+$ ions (admicelles, dimers) will be formed [14, 18, 19].

Thus, clearly that cationic surfactant- $CaCO_3$ nanoparticles interactions and the structure that form a consequences of these interactions, critically determine the phase behavior of the shell wall-structure covering the nanoparticles and possibly the nanoparticles dispersion. But, only a few research works involve in investigating CTAB molecules (cationic surfactant) adsorp into hydrophilic $CaCO_3$ nano-cube particles especially under alkaline condition in preparation of covering the $CaCO_3$ nanoparticles with meso-structure shell wall. This initial investigation of the $CaCO_3$ nanoparticles surface coating in aqueous medium enables to understand the industrial coating process of the nanoparticles under alkaline condition. This paves the way also in improving the knowledge of the effect of other organic surfactant coating on the interface adhesion between the matrix and $CaCO_3$ nanoparticles under alkaline condition.

Hence in this chapter, the cationic surfactant cetyltrimethyammonium bromide (CTAB) was selected in this experiment to determine the adsorption onto hydrophilic $CaCO_3$ nanoparticles. thermogravimetric analysis (TG-DTA), raman spectroscopy, Scanning-Transmission electron microscope (STEM-TEM), N_2 adsorption –desorption isotherm, gas chromatograph combined with mass spectrometer (GC-MS) and powder X-ray diffraction pattern (PXRD) were determine as functions of concentration of certain cationic surfactant to obtain initial evidence about the mechanism of adsorption of hydrophilic $CaCO_3$ nanoparticles under alkaline condition.

4.2 Materials and schematic outline

4.2.1 Materials

Nano-cube 60 Calcium carbonate ($CaCO_3$, RMHA) (Nittetsu Kogyo) was used as core particles while, hexadecyltrimethylammonium bromide (CTAB, 99% Nacalai

Tesque, Inc.) as cationic surfactant, adsorp by hydrophilic $CaCO_3$ nanoparticles forming micro/mesoporous shell wall. Ammonia water (NH_4OH, 28% Wako pure chemical) used as alkaline conditioning and distilled water (H_2O)/Ethanol (EtOH, 99% Wako pure chemical) used as a solvent for the template adsorption.

4.2.2 Preparation process for the adsorption of CTAB molecules onto $CaCO_3$ nanoparticles under alkaline-aqueous condition

Preparing for the adsorption of CTAB molecules onto $CaCO_3$ nanoparticles under alkaline condition is the same procedural approach in Chapter 3.1.1 except for the addition of TEOS. In this case, CTAB concentration (y mM; millimolar) was dissolved in deionized water (H_2O) by magnetic stirrer at R.T until becomes clear solution (CTAB solution, y mM). Separately, nano-size $CaCO_3$ mixed with ethanol (EtOH) by magnetic stirrer for about 15 minutes ($CaCO_3$ solution). Then, CTAB solution (y mM) and $CaCO_3$ solution were combined under stirring for about 1 h at R.T (y mM/$CaCO_3$). Next, NH_4OH (28%) was added to the y mM/$CaCO_3$ solution under vigorous stirring. Then white solution continuously mixed and stirred for 24 h at R.T with the final general molar ratio of ($CaCO_3$:EtOH:H_2O:NH_4OH:CTAB = 1:8.38:20.8:0.94:0.043) if the 57.02mM CTAB concentration is used. After 24 h continuous stirring, the white gel solution was centrifuged. After then, separate the liquid and solid particles in a separate container. The solid samples were dried in a vacuum oven to 90 °C for 5 h. Then ready for the characterization. The process flow is shown in Figure 4.1.

(Note: CTAB concentration (y mM = 0.04 mM to 88.52 mM; denoted as y mM/$CaCO_3$) is only varied to optimized the investigation of the adsorption of CTAB molecules onto $CaCO_3$ nanoparticles under alkaline condition)

4.2.3 Physico-chemical characterization

The product were characterized by X-ray Diffraction (XRD, Model RINT 1100, Rigaku) with Cu Kα radiation (λ= 1.54056 Å), with scanning speed of 0.05° and scanning length of 0.02 °/ s at a small angle (5 ° to 60 °, 2θ) with an operating voltage of 40 kV and emission current 40 mA.

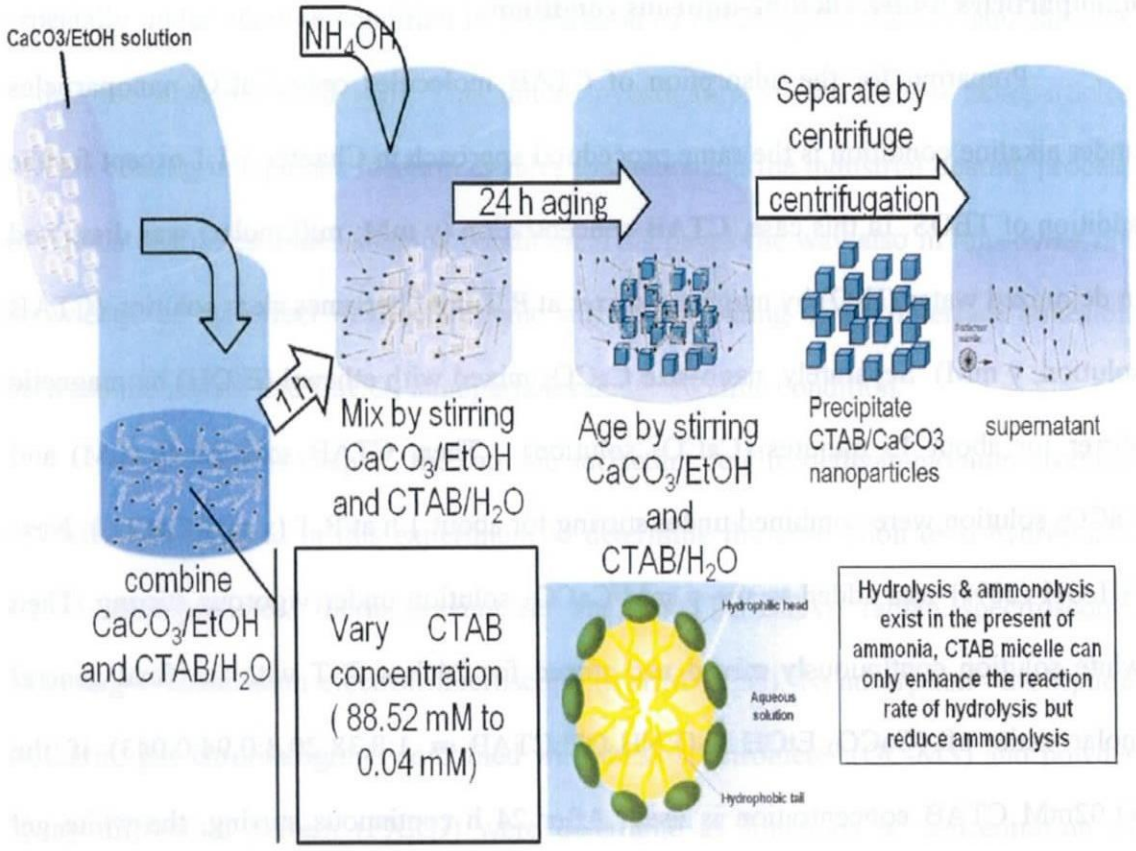

Figure 4. 1 Process flow in preparing for the adsorption of CTAB molecules onto $CaCO_3$ nanoparticles under alkaline condition

Raman spectrometer applied (JASCO NRS-3100) was equipped with a YAG laser (power 2.3 mW, wavelength 532 nm). Samples were exposed for 2 min and spectra were taken at random places on the surface of each sample (for better reproducibility). Spectra frequency reported to $\pm 2cm^{-1}$. The spectra of pure solid and

concentrate CTAB/solid were spread uniformly to the special glass slide for measurements

GC-MS analysis was performed using gas chromatograph combined with mass spectrometer GCMS-QP2010 Ultra/SE (Shimadzu Kyoto, Japan) set with Rtx-5MS capillary column (30 m length, 0.25 mm i.d, 0.25 μm film thicknes). The oven temperature was kept at 150 °C. The ion source and transfer line were kept at 200 °C to 300 °C. GCMS analysis was realized using electron ionization 70 V within (m/z = 35 to 400) for CTAB molecules confirmation. The powder samples were analyze by direct method by firstly decomposed at 150 °C (then analyze) and finally decomposed it 300 °C (then analyze). In this case, two data's of GCMS were obtained in order to clarify and carefull identify the CTAB molecules. Each temperature decomposition`s had a total run time of 30 min.

The thermal property of the sample was investigated using the Thermogravimetry (TG, TG-8120, Rigaku, Japan) under oxygen atmosphere. The heating rate of the temperature increase at 10 °C/min with temperature ranged from (22 to 1000) °C. Morphology particles were examined using scanning electron microscopy (STEM; JSM-7000F, JEOL) and transmission electron microscopy (TEM, 2000EXII). In STEM and TEM observation, the samples were dispersed in ethanol ultrasonically and were dropped into the copper grid. The specific surface area was calculated by Brunauer-Emmett-Teller (BET) method via the automatic surface area analyzer (BELSORP-max) with Nitrogen gas adsorption and desorption isotherm recorded at 77K.

4.3 Results and discussions

On the basis of the qualitative and quantitative analyses based on the TGA/DTA, GCMS and STEM/TEM characterization on the $CaCO_3$ nano-cube particles coated with cationic surfactant CTAB molecules in aqueous medium under alkaline condition and references similar to the researcher study, the adsorption process on the cationic self-assembled molecules on the hydrophilic $CaCO_3$ nano-cube particles is discussed in the following part

4.3.1 Crystallographic /Morphological properties

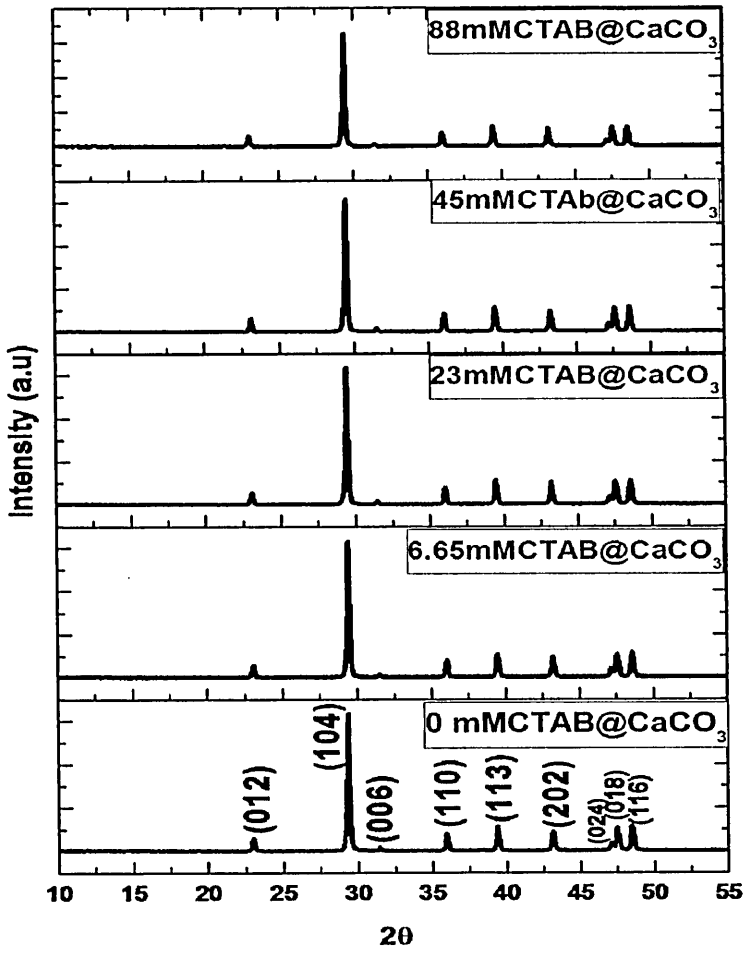

Figure 4.2 XRD pattern of raw $CaCO_3$ nanoparticles with different CTAB concentration adsorp onto $CaCO_3$ nanoparticles

The XRD patterns of the different CTAB (mM) concentration to be absorbed by $CaCO_3$ nano-cube particles in an aqueous medium under alkaline condition were illustrated in Figure 4.2. All the samples (CTAB/$CaCO_3$ nanoparticles) showed a diffraction angle identified as calcite (core nanoparticles $CaCO_3$) a cubic unit cell.[20, 21]. It is noteworthy that XRD pattern indicates no change in the unit cell parameters or no characteristic peaks of other impurities are observed as concentration of CTAB increase under alkaline condition as shown in Figure 4.2. It indicates that all the samples were cubic-calcite nano-structure particles despite the increase addition of CTAB concentration onto $CaCO_3$ nanoparticles. This XRD analysis shows that the sharp reflection peaks indicate a crystalline structure of the cubic $CaCO_3$ which signify that the CTAB molecules adsorbed in the core nanoparticles.

In this case as predicted, morphology of $CaCO_3$ nanoparticles was not affected by rapid mixing/ultrasonic and adsorption of increasing CTAB concentration at ambient temperature under continuously stirring for 24 h in an alkaline condition as clearly observed at SEM/TEM images shown in Figure 4.3. The nano-sized CTAB/$CaCO_3$ composite samples (at increasing CTAB concentration) with uniform cubic shape and monodisperse nanoparticles were observed (see Figure 4.3a to 4.3f). This nano-cubic morphology for the adsorption of CTAB on $CaCO_3$ nanoparticles was preserved. No clear aggregates were also observed. All samples with cubic-like crystals of more less 60 nm were obtained as revealed by the TEM micrographs in Figure 4.3(e & f). Though the TEM images (Figure 4.3e and 4.3f) cannot observe the critical micelle concentration (CMC) at this point/results, but thin layers of CTAB (consist of layers of hemimicelles, admicelles, bilayer, and admicelles) [22] adsorbed on $CaCO_3$ nanoparticles was detected

especially in 88 mM CTAB/$CaCO_3$ nanoparticles as shown in Figure 4.3f. This correlation between the stability of the particle morphology with attached surfactant (cationic-organic) is important aspect in concluding the compatibility of the cationic surfactant and adsorption distribution of the hydrophilic $CaCO_3$ nanoparticles are obviously possible. This layer of CTAB molecules adsorb onto the $CaCO_3$ nanoparticles may play an important role during the formation of mesophase layer onto the $CaCO_3$ nanoparticles upon addition of inorganic precursors such as metal alkoxides or aqueous silicon alkoxides.

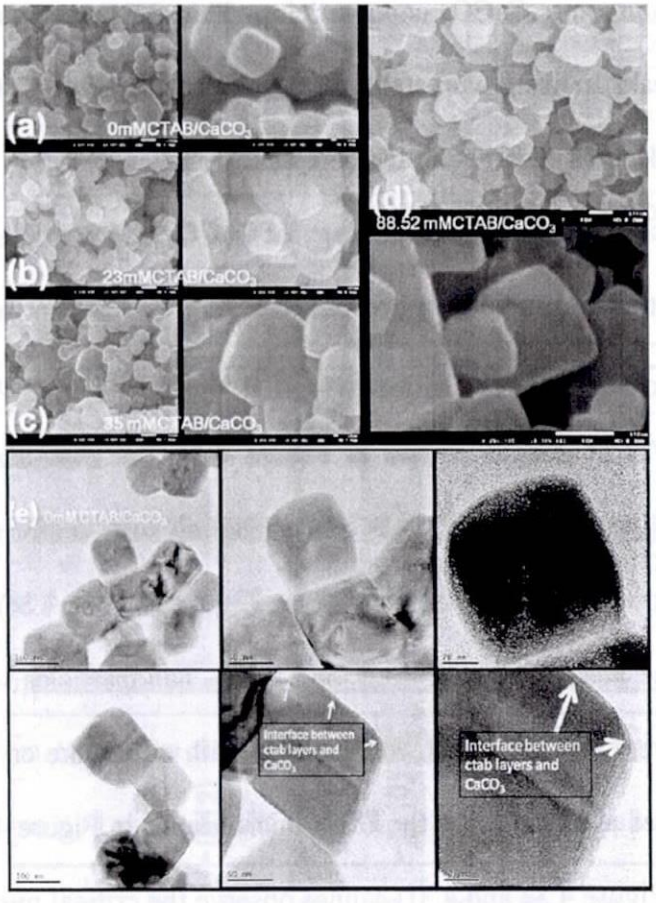

Figure 4. 3 SEM and TEM images of raw $CaCO_3$ nanoparticles (a, e) with different CTAB concentration such as 23 mM CTAB (b), 35 mM CTAB (c), 88 mM CTAB (c and d) sample.

4.3.2 Raman and GCMS Analysis

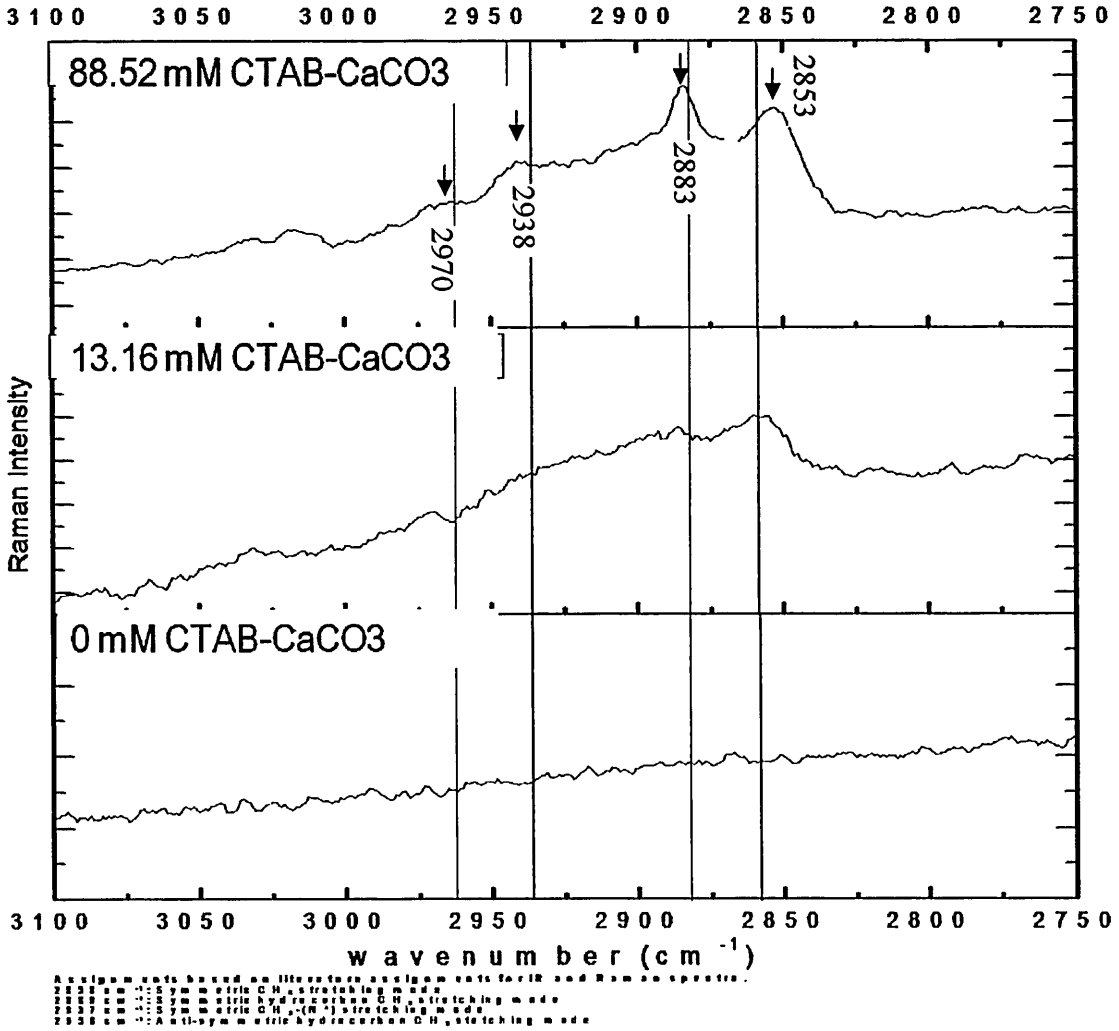

Figure 4. 4 The C-H stretching region in the Raman spectra of CTAB adsorbed on $CaCO_3$ nanoparticles from 0 mM CTAB-$CaCO_3$ (raw material), 13.16 mM CTAB-$CaCO_3$ and 88 mM CTAB-$CaCO_3$.

In order to check the CTAB (cationic surfactant) molecules was adsorbed onto the surface of the $CaCO_3$ nanoparticles in an aqueous solution under alkaline condition, the Raman and GC-MS analysis were employed as shown in Figure 4.4 and 4.5 respectively. Raman Scattering is not intrinsically surface sensitive and detects the contribution of the $CaCO_3$ nanoparticles (substrate) as well as from the adsorbed

surfactant layer. In Figure 4.4 show Raman spectrum of the C-H stretching modes from 2750 – 3100 cm^{-} for CTAB adsorbed on the $CaCO_3$ nanoparticles (88 mM and 13.16mM CTAB/$CaCO_3$) and compared with raw $CaCO_3$ nanoparticles (0 mM CTAB/$CaCO_3$). (Note: Strong peaks below 1300 cm^{-} are from the $CaCO_3$ nanoparticles [23-25], see Figure 4.S1). As expected, C-H stretching modes of the CTAB appeared between 2800 -3000 cm^{-} [26] while raw $CaCO_3$ nanoparticles (0 mM CTAB/$CaCO_3$) no peak was observed. In the rest of this section, discussion is concentrated on the structural sensitive of C-H-modes. The assignments of the majority of peaks observed in this spectra region are well established already.[22, 26-28]. The strongest bands originate from the methylene stretches; specifically the antisymmetric methylene at approximately around 2883 cm^{-}, the symmetric methylene stretch at 2853 cm^{-} and some broad peaks at 2938 – 2970 cm^{-} is tentatively assigned to an overtone of terminal alkyl chain CH_3 deformation [22, 27, 29-31]. These CH-stretching frequency patterns obviously increase as concentration of CTAB. Hence, the methyl groups from the surfactant headgroups are largely responsible for these intensities of these bands which are normally assigned to long-chain methylene asymmetric and symmetric stretching motions[22]. The CH_2 stretching modes are generally the most intense features observed because the widths and frequency of these vibrational modes are sensitive to the *gauche/trans* conformer ratio of the surfactant tails.[27, 28]

To detect CTAB molecule was attached even at low concentration of CTAB adsorbed onto $CaCO_3$ nanoparticles, GC-MS analysis was used. It was realized using electron ionization 70 V within (m/z = 35 to 400) for CTAB confirmation.

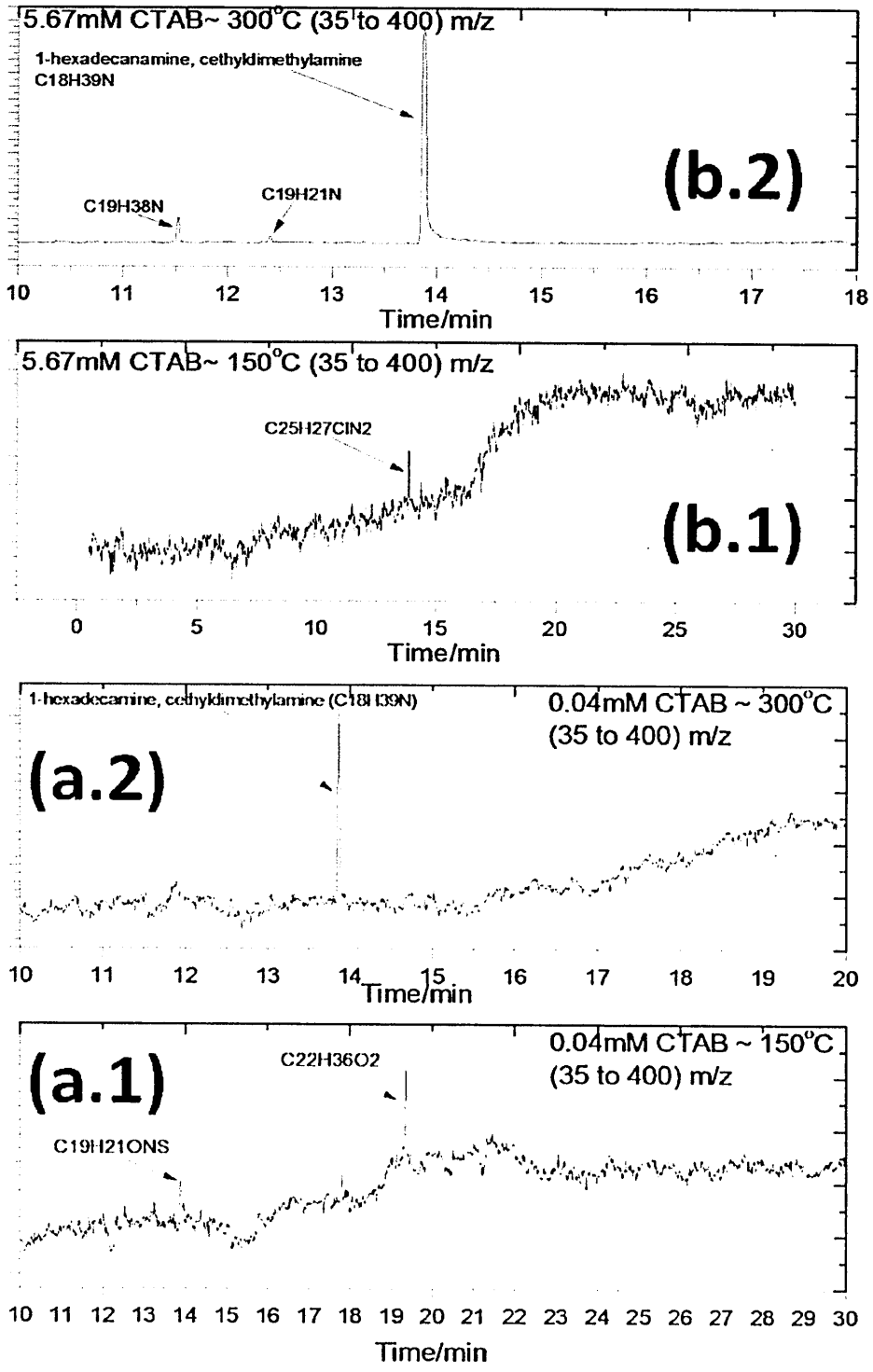

Figure 4. 5 GC-MS analysis of ([a] 0.04 mM and [b] 5.67mM) CTAB/$CaCO_3$ samples degradation temperature at (a.1 &b.1) 150 °C and (a.2 &b.2) 300 °C

The composition of the condensate obtained from the samples containing low concentration of surfactant CTAB (0.04 mM and 5.67 mM) adsorbed onto the nano $CaCO_3$ particles processed at 150°C and 300°C was shown in Figure 4.5. This data was compared with the pure CTAB powder as shown in Figure 4.S2. Composition $C_{22}H_{36}O_2$ may form at 150 °C present in both (0.04 mM and 5.67 mM) CTAB/$CaCO_3$ as shown in Figure 4.5 (a1 and b1).

However, the composition of the CTAB/$CaCO_3$ condensate at 300°C is more complex. As it is seen there were three major peaks found especially in the 5.67mMCTAB/$CaCO_3$ sample (Figure 4.5b2) which describe as 1-hexadecanamine ($C_{18}H_{39}N$), $C_{19}H_{38}N$ and $C_{19}H_{21}N$ [32]while for the sample 0.04 mMCTAB /$CaCO_3$, only 1-hexadecanamine was present. Then, it can be stressed out that the liberation of $C_{22}H_{36}O_2$ and 1-hexadecanamine is related to desorption of CTAB onto the nanosize $CaCO_3$ particles. In general, even at low concentration CTAB adsorption is still possible because of the partial decomposition of the CTA^+ observed in the GC-MS analysis

4.3.3 Thermal Analysis

The thermal properties/calorimetric behavior of the CTAB coated $CaCO_3$ was scanned at (25 to 1000) °C at the rate of 10°C/min. Then adsorbed amount of CTAB molecules, which is determined by the weight loss in TGA experiments, together with peak area under DTA which is the enthalpy change (ΔH) [33, 34] of the CTAB/$CaCO_3$ samples during the adsorption and the decomposition of $CaCO_3$ nanoparticles were reported in Table 4.1 and shown in Figure 4.6, 4.7 and 4.8.

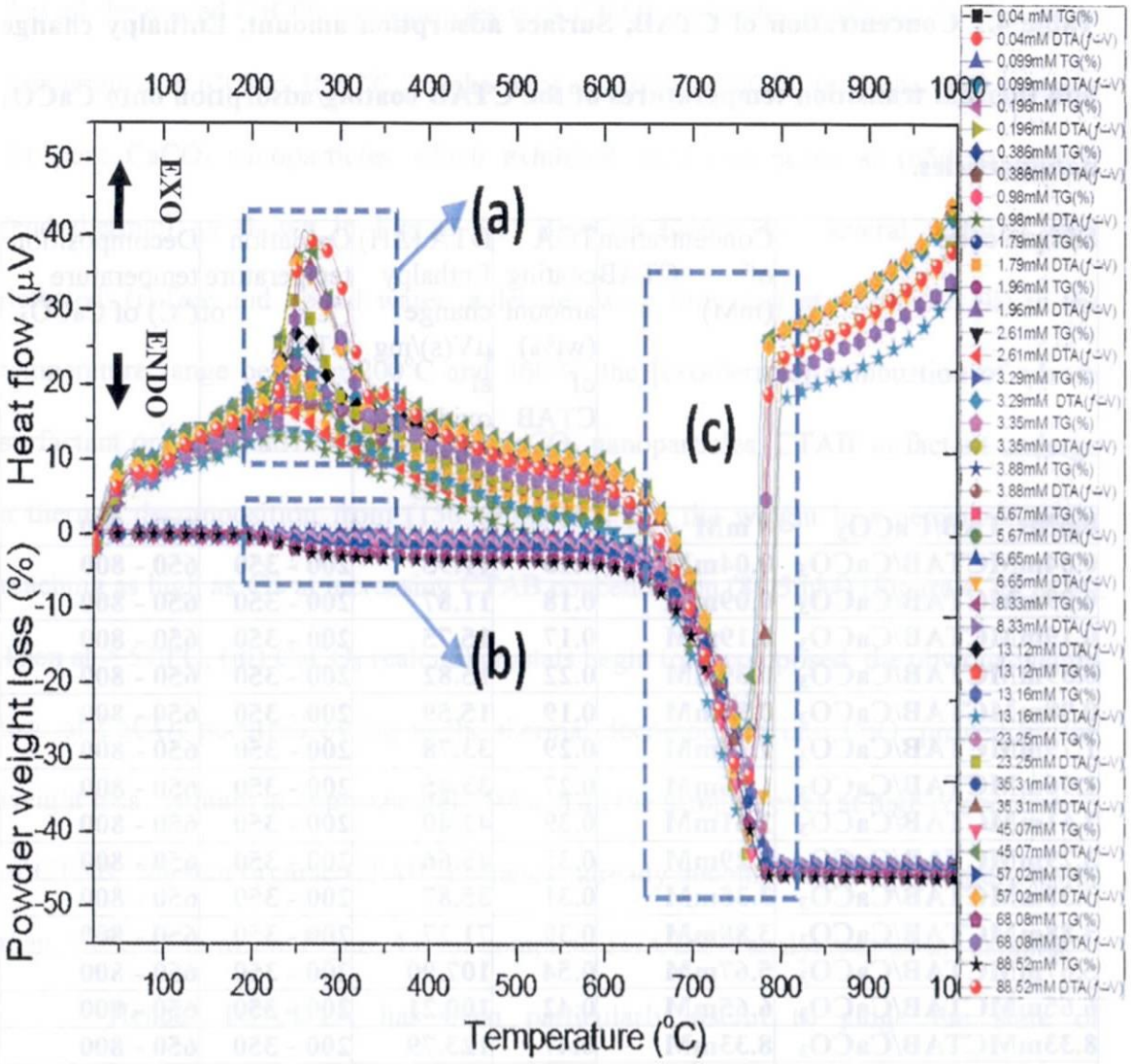

Figure 4.6 Complete TG-DTA analysis of the CTAB adsorption at increasing concentration (mM) onto $CaCO_3$ nanoparticles under alkaline condition

Table 4.1 Concentration of CTAB, Surface adsorption amount, Enthalpy change and thermal transition temperatures of the CTAB coating/adsorption onto $CaCO_3$ nanoparticles.

Sample code	Concentration of CTAB (mM)	TGA coating amount (wt%) of CTAB	DTA (ΔH) Enthalpy change μV(s)/mg at oxidation temp of CTAB	Oxidation temperature (°C) of CTAB	Decomposition temperature (°C) of $CaCO_3$
0mMCTAB/$CaCO_3$	**0 mM**	-	-	-	**650 - 800**
0.04mMCTAB/$CaCO_3$	**0.04mM**	**0.13**	**11.95**	**200 - 350**	**650 - 800**
0.09mMCTAB/$CaCO_3$	**0.09mM**	**0.18**	**11.87**	**200 - 350**	**650 - 800**
0.19mMCTAB/$CaCO_3$	**0.19mM**	**0.17**	**15.75**	**200 - 350**	**650 - 800**
0.39mMCTAB/$CaCO_3$	**0.39mM**	**0.22**	**15.82**	**200 - 350**	**650 - 800**
0.98mMCTAB/$CaCO_3$	**0.98mM**	**0.19**	**15.59**	**200 - 350**	**650 - 800**
1.79mMCTAB/$CaCO_3$	**1.79mM**	**0.29**	**33.78**	**200 - 350**	**650 - 800**
1.96mMCTAB/$CaCO_3$	**1.96mM**	**0.27**	**33.45**	**200 - 350**	**650 - 800**
2.61mMCTAB/$CaCO_3$	**2.61mM**	**0.39**	**42.40**	**200 - 350**	**650 - 800**
3.29mMCTAB/$CaCO_3$	**3.29mM**	**0.35**	**45.66**	**200 - 350**	**650 - 800**
3.35mMCTAB/$CaCO_3$	**3.35mM**	**0.31**	**35.87**	**200 - 350**	**650 - 800**
3.88mMCTAB/$CaCO_3$	**3.88mM**	**0.39**	**71.27**	**200 - 350**	**650 - 800**
5.67mMCTAB/$CaCO_3$	**5.67mM**	**0.54**	**107.90**	**200 - 350**	**650 - 800**
6.65mMCTAB/$CaCO_3$	**6.65mM**	**0.42**	**100.21**	**200 - 350**	**650 - 800**
8.33mMCTAB/$CaCO_3$	**8.33mM**	**0.47**	**123.79**	**200 - 350**	**650 - 800**
13.1mMCTAB/$CaCO_3$	**13.1mM**	**0.68**	**135.66**	**200 - 350**	**650 - 800**
13.2mMCTAB/$CaCO_3$	**13.2mM**	**0.65**	**144.43**	**200 - 350**	**650 - 800**
23.3mMCTAB/$CaCO_3$	**23.3mM**	**0.77**	**170.13**	**200 - 350**	**650 - 800**
35.3mMCTAB/$CaCO_3$	**35.3mM**	**1.49**	**289.89**	**200 - 350**	**650 - 800**
45.1mMCTAB/$CaCO_3$	**45.1mM**	**1.59**	**325.35**	**200 - 350**	**650 - 800**
57.02mMCTAB/$CaCO_3$	**57.02mM**	**1.47**	**300.18**	**200 - 350**	**650 - 800**
68.1mMCTAB/$CaCO_3$	**68.1mM**	**2.69**	**286.14**	**200 - 350**	**650 - 800**
88.5mMCTAB/$CaCO_3$	**88.5mM**	**3.09**	**316.43**	**200 - 350**	**650 - 800**

Recently, several researchers [18, 35, 36] used TGA/DTA analysis to determine the (surfactant) adsorption molecules on the inorganic carbonates (ex. $CaCO_3$ nanoparticles) which were prepared in a solvent medium. The complete TGA/DTA traces of the increase CTAB concentration adsorp on the $CaCO_3$ nanoparticles; showed

that all the coated $CaCO_3$ nanoparticles with CTAB molecules exhibited the two peaks temperatures at (200 to 350) °C [exothermic] and (650 to 800)°C [endothermic] except for pure $CaCO_3$ nanoparticles which exhibited only one peaks at (650 to 800)°C [endothermic] as shown in Figure 4.6. Base on Figure 4.6, several features were detected: (i) free and bound water molecules were fully lost at < 200 °C; (ii) in the temperature range between 200°C and 360°C, the [exothermic] combustion of adsorb surfactant organic matrixes onto cubic $CaCO_3$ nanoparticles. CTAB surfactant undergo a thermal decomposition from (150 to 400°C), and the weight loss percent increase reaching as high as 4% at increasing CTAB concentration (88.5mM) (Figure 4.7(a & b)). Then at > 570°C, (iii) $CaCO_3$ (calcite) crystals begin to decomposed, the obvious weight loss of $CaCO_3$ occurred owing to the thermal decomposing into CaO; proven by the weight loss maintain at approximately 50% in all the samples even at high concentration of CTAB, wherein organic CTAB substances already decomposed at temperature lower than 350°C as shown in Figure 4.6 for complete TGA/DTA analysis of all the samples.

Hence, TGA/DTA has been particularly useful to judge the state of adsorption[35, 37]. Technically, adsorption of CTAB on the surface of cubic $CaCO_3$ nanoparticles, the combustion and loss of the surfactant molecules adsorbed on the cubic $CaCO_3$ nanoparticles took place at about 240°C to 250°C even if the CTAB concentration increase which was directly observe3d in Figure 4.7 (a & b). These dense packed CTAB molecules are expected to be difficult to wash out, even if it is not chemically bound[35]. Since, the adsorption of alkaline rich-CTAB molecules onto NcCP did not alter the calcite structure based from the XRD data, SEM, and TEM

analysis (Figure 4.2 and 4.3 respectively). Thus, it can be affirmed that cubic $CaCO_3$ nanoparticles is fairly suitable as an adsorbent for cationic organic substances.

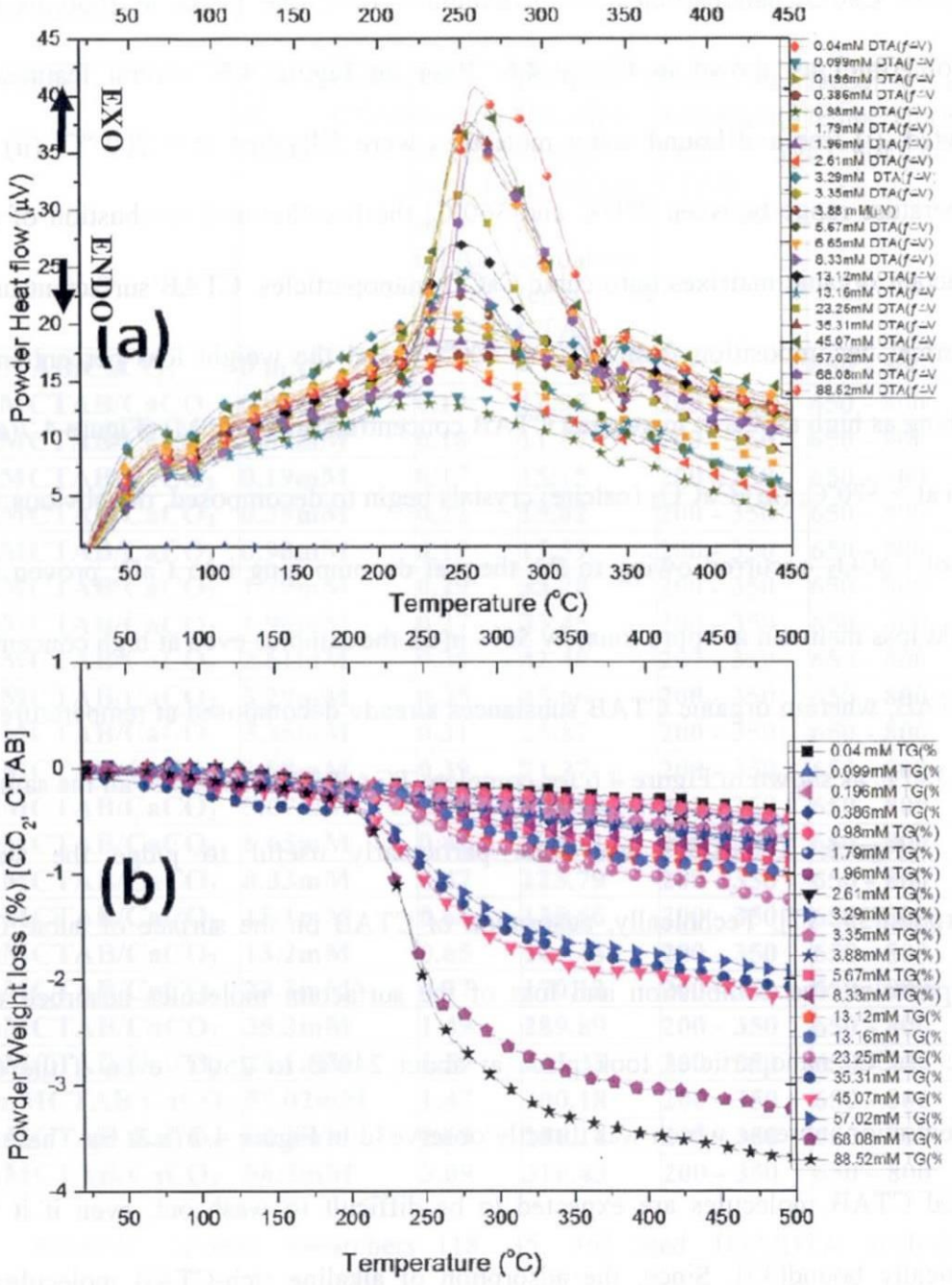

Figure 4. 7 DTA (b) and TG (a) analysis at 25°C to 500°C CTAB adsorption at increasing concentration (mM) onto $CaCO_3$ nanoparticles under alkaline condition

4.3.4 Relationship between heat change enthalpy of dehydration for CTAB and actual adsorption isotherm of the dried precipitate CTAB/$CaCO_3$

The relationship between the transition (decomposition; 200°C to 400°C) enthalpy for the CTAB layers adsorbed on the nano-cube $CaCO_3$ particles (NcCP) surfaces versus the adsorbed amount of CTAB determined by TGA measurements was presented in Figure 4.8a. As shown in the graph, decomposition enthalpy approximately elevate linearly as the adsorbed amount of CTAB concentration increase (up to less than 1.8%, calculated full monolayer coverage) onto NcCP surface (see Figure 4.8b and Figure 4.S3 and 4.S4). Because decomposition peak in the DTA measurements majority belongs to the physically adsorbed CTAB layers, it means that the physically adsorbed part increases in a proportional way to the total organic amount of surfactant. From the slopes lines in Figure 4.8a, an estimation of the dehydration/decomposition enthalpy for the physisorbed CTAB layers is about -14.706 μVs/mg (-16.6 J/g; 1μVs/mg =1.129 mJ/mg [38]) approximately around -6.06 kJ/mol. For comparison with literature, the values approximately around (-2.60 to -12) kJ/mol for enthalpy of CTAB formations [39, 40], even though with different techniques.

While in Figure 4.8b, It showed the relationship between adsorp (weight percentage loss) CTAB (200 to 400 °C, CTAB decomposition only and 25 to 400 °C, dehydration and decomposition) versus original amount of increasing NH_4+-CTAB concentration. In this case, the adsorbed amount of CTAB, was determined by the weight loss in TGA experiments at (200 to 400)°C, together with the original amount of CTAB added during the coating/adsorb process in NH_4+-aqueous ethanol solution was reported in Table 4.1.

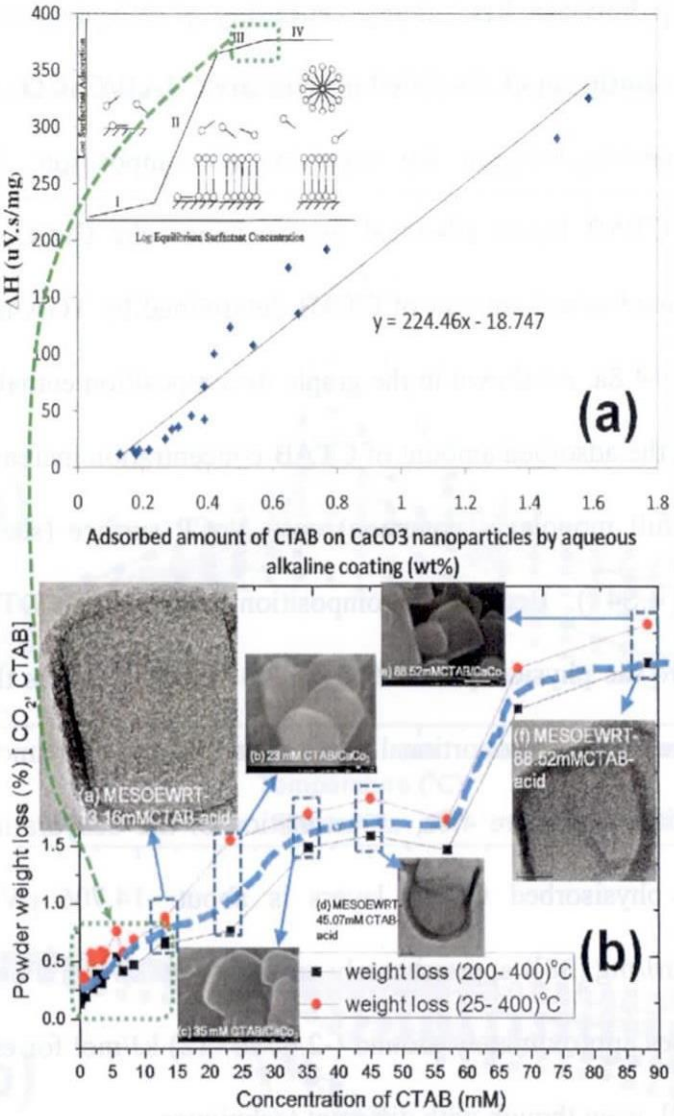

Figure 4. 8 Relationship between (a) heat change of enthalpy of dehydration of CTAB, peaks (using DTA) vs adsorbed content of CTAB onto nano-cube $CaCO_3$ particles (using TGA). (inset (a), adsorption isotherm (general) and molecular model for four step adsorption models [22]. Then (b), relationship between weight loss of CTAB adsorp onto nanocube $CaCO_3$ nanoparticles vs original (NH_4+) -CTAB concentration with TEM/SEM images based on the previous results in Chapter 3. (inset (b) green mark is the assume calculated percentage amount of CTAB monolayer coated /adsorbed onto nanocube $CaCO_3$ nanoparticles and assume to be in region III marked at inset (a)).

There were some abnormalities of the adsorption isotherm graph as compared to the references [22, 41], maybe due to an imperfect control of the process during surface coating and also mainly on the difference of characterization techniques. But anyway, this version of adsorption isotherm graphs clearly indicates the cationic CTAB added during coating process was adsorbed to the aqueous $EtOH/H_2O$- (NH_4+)-NcCP solution. In the literature, the exact determination of the surface area covered by one molecules of CTAB at the equilibrium is one important parameter [42]. Some researchers indicated the parameters depending on the morphology of the particles. For example, if the cross-sectional area of CTAB molecules assumed to be 0.64 nm^2, which corresponds to the surface area for one CTAB molecules in a perpendicular orientation [43, 44], for the mean surface area (s.a) of NcCP used in this work (actual s.a, 12.05 m^2/g, Figure 4.S4), the theoretical full monolayer coverage is about 1.14% (mark as shown in Figure 4.8b). However, in the actual coating process in aqueous $(EtOH/H_2O)$ (NH_4+) medium, the adsorbent amount CTAB molecules increases even beyond the theoretical monolayer coverage, as shown in Table 4.1, Figure 4.8 (a & b). In other words, the CTAB layers formed on the NcCP surface must probably exist in a multilayer forms instead of only a monolayer form, with the number of layers increasing as adsorbed amount of CTAB concentration increases. This was clearly shown in the TEM results of Chapter 3 upon the addition of TEOS, wherein wormhole pattern can be clearly observed. Hence, TEM images of MESOEWRT 13mM, could be in between region II and III, above the monolayer coating as shown in inset Figure 4.8b-(a). Then, when CTAB adsorption is saturated already the excess CTAB molecules would be in the solution, visually

observed in TEM image of MESOEWRT 88 mM, thickness of mesophase is roughly the same with low concentration of CTAB.

4.3.5 Plausible Mechanism for the adsorption of CTAB molecules onto hydrophilic $CaCO_3$ nanoparticles then form a wormhole mesoporous pattern

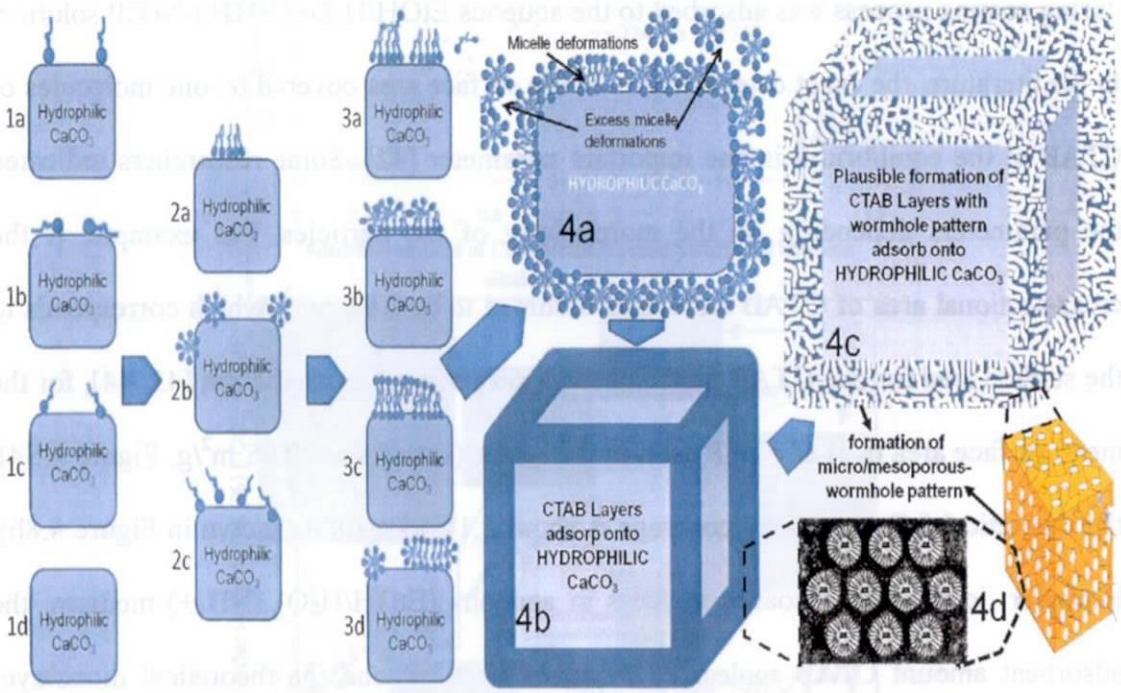

Figure 4. 9 Schematic illustration displaying morphologies that may form /occur during the adsorption of soluble cationic surfactant to a hydrophilic $CaCO_3$ nano-cube particle (substrate) (1d). and the formation of micro/mesoporous wormhole pattern on the surface of hydrophilic $CaCO_3$ nano-cube particle

Based from the reported data and references, the adsorption of CTAB onto NcCP/aqeous ($EtOH/H_2O$)-NH_4 interface mainly takes place through ion exchange, the ion pairing and hydrophobic bonding. The predominant mechanisms in the lower CTAB concentrations are probably ion exchange and ion pairing. The hydrophobic bonding mechanism predominates with the increasing CTAB concentration. It can be determined

that the signs of isosteric adsorption enthalpy (ΔH) for adsorption of CTAB onto hydrophilic NcCP are negative and positive, respectively. As CTAB concentration increases up to 88.5 mM, the amount of CTAB adsorbed increase indicating the exothermic nature of adsorption process. This verifies the negative sign expected of (ΔH_{ads})[45]. As results of this adsorption, Figure 4.9 illustrate the schematic plausible mechanism may form /occur during the adsorption of soluble cationic CTAB to a hydrophilic NcCP (substrate) (1d). At very low concentration, the hydrocarbon chains of the adsorbed surfactant may be lie perpendicular to the surface (1a), parallel to the surface (1b), or randomly distributed (1c), As the concentration increase, between surfactant molecules may be lead to the formation of hemimicelles (2a) or admicelles (2b). At high concentration, a range of structures are conceivable such as monolayer (3a), hemimicelles on the monolayer (3b), bilayer (3c), or admicelles (3d). Thereby, the possible explanation for the formation of micro/mesoporous wormhole pattern film (4c, 4d) onto the surface of NcCP.

Based from referred papers and experimental data, coating process of NcCP by cationic (CTAB) surfactant in aqueous medium resulted into multilayers of surfactant that can be individualized into two basic types. One is the chemisorbed monolayer directly on the NcCP. The other one consist of one or more physisorbed layers of admicelles or hemimicelles. This first layers is connected with the monolayer through a (chemical or electrostatic interaction) weak interface link between the hydrocarbons chains in a tail-to tail arrangement. With the presence of aqueous ($EtOH/H_2O$) NH_4+, CTAB micelle can only enhance the reaction rate of hydrolysis but reduce ammonolysis [46] without affecting the structure of NcCP (substrate) and the adsorption capacity.

Taking into account the limited information of this study, the plausible CTAB adsorption onto hydrophilic NcCP has been proposed for the aqueous coating process under alkaline condition. Then, rationalization for the formation/growth of physicorbed CTAB molecules as multilayer which eventually when saturation occur form excess micelles (4a, Figure 4.9)

Hence with precise amount of CTAB concentration, formation of wormhole micro/mesoporous pattern phase onto NcCP (nanosize $CaCO_3$) can be possible explained by the following reasonable justification: (1) aside from it's in nano-size, NcCP as inorganic template has due high surface energy, thereby adsorb the surfactant CTAB molecules. Then enriched onto the surface NcCP, wherein the CTAB concentration on the surface of NcCP is higher than that in bulk liquid phase, reaching the second micelle concentration (cmc2) forming layered CTABS (micro/mesoporous wormhole pattern) (4b, 4c,4d). (2) In this case, CTAB surfactant will be roughly perpendicular to the surface of NcCP by means of complicated synergistic effects such as weak non-covalent bond of smaller directionality includes coulombs force, hydrogen bond, steric hindrance, van der walls force, weak ionic bond or ionic strength and forms disordered hexagonal array in a wormhole pattern through self-assembly [47, 48]. (3) Since its in alkaline condition (hydrolysis and ammonolysis exist [46]), an addition of liquid metal oxide precursor such as TEOS a silicon sources can be hydrolyzed to generate silicic acid oligomers having multiple coordination's sites, then fills , agglomerates and deposits around the framework of disordered hexagonal array micelles (worm hole pattern) to generate the shell thickness (4c,4d). (4) Removing the organic surfactant (CTAB) thru calcinations or acid treatment, can generate novel

micro/mesoporous wormhole pattern channel with hollow nanoparticles (note: NcCP easily dissolved by acid etching) as shown in Figure 6 (4d).

However, the exact reasons needs to be further investigated and elucidated. This model of the hydrophilic NcCP surface coating in (NH_4+)-aqueous coating process enables to better understand the meso-phase industrial coating process of hydrophilic NcCP and paves the way for an improve knowledge of the effect of the organic surfactant coating on the interface adhesion between the matrix and NcCP in the polymeric composites.

4.4 Conclusion

In this chapter, the researcher has demonstrated/illustrated an initial investigation on the adsorption of (cationic surfactant) CTAB molecules onto the $CaCO_3$ nanoparticles under alkaline condition based on the TGA/DTA, GCMS and STEM/TEM data. It has presumable/comparable results based on the general notion for the adsorption of surfactant on the hydrophilic surface'($CaCO_3$ particles has hydrophilic surface[41, 49]). The researcher has used various references, calculated, and experimental results on the adsorption of CTAB covering the $CaCO_3$ nanoparticles in alkaline condition. Based from referred papers and experimental data, coating process of $CaCO_3$ nanoparticles by cationic (CTAB) surfactant in aqueous medium resulted into multilayers of surfactant that can be individualized into two basic types. One is the chemisorbed monolayer directly on the $CaCO_3$ nanoparticles. The other one consist of one or more physisorbed layers of admicelles or hemimicelles. This first layers is connected with the monolayer through a (chemical or electrostatic interaction) weak interface link between the hydrocarbons chains in a tail-to tail arrangement. The

maximum amount of CTAB adsorbed on the $CaCO_3$ nanoparticles under alkaline condition is determined to be about by mneans of TGDTA technique. This result can be confirmed by the calculated adsorption of CTAB onto the $CaCO_3$ nanoparticles using the actual surface area of $CaCO_3$ nanoparticles and the given theoretical head area of CTAB molecules. Taking into account the limited information of this study, the plausible CTAB adsorption onto hydrophilic $CaCO_3$ nanoparticles has been proposed for the aqueous coating process under alkaline condition and this can explain both the formation of incomplete monolayer and growth of physicorbed CTAB molecules as multilayer which eventually when saturation occur form excess micelles. However, the exact reasons needs to be further investigated and elucidated. But theoretically, this proves that the advantage of nanoparticles is the high surface area per gram of materials, so that the absorbance of surface species (CTAB molecules) is relatively strong at a sufficient amount of surfactant. This model of the hydrophilic $CaCO_3$ nanoparticles surface coating in aqueous coating process under alkaline condition enables to better understand the industrial with mesophase coating process of hydrophilic $CaCO_3$ nanoparticles and paves the way for an improve knowledge of the effect of the organic surfactant coating on the interface adhesion between the matrix and $CaCO_3$ nanoparticles in the polymeric composites.

References

[1] D. Myers, Surfaces, interfaces, and colloids: principles and applications, Wiley-VCH, 1999.

[2] S. Beach, J. Newsted, K. Coady, J. Giesy, Ecotoxicological Evaluation of Perfluorooctanesulfonate (PFOS), in: L.A. Albert, P. Voogt, C.P. Gerba, O. Hutzinger, J.B. Knaak, F.L. Mayer, D.P. Morgan, D.L. Park, R.S. Tjeerdema, D.M. Whitacre, R.S.H. Yang, G.W. Ware, H.N. Nigg, D.R. Doerge, F.A. Gunther (Eds.) Reviews of Environmental Contamination and Toxicology, Vol. 186, Springer New York, 2006, pp. 133-174.

[3] Z.G. Cui, L.L. Yang, Y.Z. Cui, B.P. Binks, Effects of Surfactant Structure on the Phase Inversion of Emulsions Stabilized by Mixtures of Silica Nanoparticles and Cationic Surfactant, Langmuir 26 (7) (2009) 4717-4724.

[4] K.P. Sharma, G. Kumaraswamy, I. Ly, O. Mondain-Monval, Self-Assembly of Silica Particles in a Nonionic Surfactant Hexagonal Mesophase, The Journal of Physical Chemistry B 113 (11) (2009) 3423-3430.

[5] L. Zhao, J. Feng, Z. Wang, synthesis and modification of calcium carbonate nanoparticles via a bobbling method, Science in China Series B: Chemistry 52 (7) (2009) 924-929.

[6] C. Wang, Y. Liu, H. Bala, Y. Pan, J. Zhao, X. Zhao, Z. Wang, Facile preparation of CaCO3 nanoparticles with self-dispersing properties in the presence of dodecyl dimethyl betaine, Colloids and Surfaces A: Physicochemical and Engineering Aspects 297 (1-3) (2007) 179-182.

[7] C. Wang, Y. Sheng, X. Zhao, Y. Pan, B. Hari, Z. Wang, Synthesis of hydrophobic CaCO3 nanoparticles, Materials Letters 60 (6) (2006) 854-857.

[8] Y.S. Han, G. Hadiko, M. FUJI, M. Takahashi, A novel approach to synthesize hollow calcium carbonate particles, Chemistry letters 34 (2) (2005) 152-153.

[9] M.F. Butler, W.J. Frith, C. Rawlins, A.C. Weaver, M. Heppenstall-Butler, Hollow Calcium Carbonate Microsphere Formation in the Presence of Biopolymers and Additives, Crystal Growth & Design 9 (1) (2008) 534-545.

[10] M. Salehi, S.J. Johnson, J.-T. Liang, Mechanistic Study of Wettability Alteration Using Surfactants with Applications in Naturally Fractured Reservoirs, Langmuir 24 (24) (2008) 14099-14107.

[11] T. Schuler, W. Tremel, Versatile wet-chemical synthesis of non-agglomerated CaCO3 vaterite nanoparticles, Chemical Communications 47 (18) (2011) 5208-5210.

[12] N. Gani, J. Khanam, Are surfactant molecules really oriented in the interface?, Journal of Chemical Education 79 (3) (2002) 332-null.

[13] V.B. Fainerman, E.H. Lucassen-Reynders, Adsorption of single and mixed ionic surfactants at fluid interfaces, Advances in Colloid and Interface Science 96 (1-3) (2002) 295-323.

[14] R.B. Bjorklund, H. Arwin, L. Järnström, Adsorption of anionic and cationic polymers on porous and non-porous calcium carbonate surfaces, Applied Surface Science 75 (1-4) (1994) 197-203.

[15] H.S. Hanna, F.Z. Saleeb, Adsorption and wetting behavior of precipitated hydroxyapatite and francolite in contact with cationic surfactants, Colloids and Surfaces 1 (3-4) (1980) 295-311.

[16] Z.G. Cui, Y.Z. Cui, C.F. Cui, Z. Chen, B.P. Binks, Aqueous Foams Stabilized by in Situ Surface Activation of CaCO3 Nanoparticles via Adsorption of Anionic Surfactant, Langmuir 26 (15) (2010) 12567-12574.

[17] Z.G. Cui, K.Z. Shi, Y.Z. Cui, B.P. Binks, Double phase inversion of emulsions stabilized by a mixture of CaCO3 nanoparticles and sodium dodecyl sulphate, Colloids and Surfaces A: Physicochemical and Engineering Aspects 329 (1-2) (2008) 67-74.

[18] X. Shi, R. Rosa, A. Lazzeri, On the Coating of Precipitated Calcium Carbonate with Stearic Acid in Aqueous Medium, Langmuir 26 (11) (2010) 8474-8482.

[19] N.I. Ivanova, E.D. Shchukin, Mixed adsorption of ionic and non-ionic surfactants on calcium carbonate, Colloids and Surfaces A: Physicochemical and Engineering Aspects 76 (1993) 109-113.

[20] J. Jiang, J. Liu, C. Liu, G. Zhang, X. Gong, J. Liu, Roles of oleic acid during micropore dispersing preparation of nano-calcium carbonate particles, Applied Surface Science 257 (16) (2011) 7047-7053.

[21] N. Nassrallah-Aboukaïs, A. Boughriet, J. Laureyns, A. Aboukaïs, J.C. Fischer, H.R. Langelin, M. Wartel, Transformation of Vaterite into Cubic Calcite in the Presence of Copper(II) Species, Chemistry of Materials 10 (1) (1998) 238-243.

[22] E. Tyrode, M.W. Rutland, C.D. Bain, Adsorption of CTAB on Hydrophilic Silica Studied by Linear and Nonlinear Optical Spectroscopy, Journal of the American Chemical Society 130 (51) (2008) 17434-17445.

[23] S.N. White, Laser Raman spectroscopy as a technique for identification of seafloor hydrothermal and cold seep minerals, Chemical Geology 259 (3-4) (2009) 240-252.

[24] S. Martinez-Ramirez, S. Sanchez-Cortes, J.V. Garcia-Ramos, C. Domingo, C. Fortes, M.T. Blanco-Varela, Micro-Raman spectroscopy applied to depth profiles of carbonates formed in lime mortar, Cement and Concrete Research 33 (12) (2003) 2063-2068.

[25] L.-G. Liu, T.P. Mernagh, Phase transitions and Raman spectra of calcite at high pressures and room temperature, American Mineralogist 75 (7-8) (1990) 801-806.

[26] S. Sun, R.L. Birke, J.R. Lombardi, Surface-enhanced Raman spectroscopy of surfactants on silver electrodes, The Journal of Physical Chemistry 94 (5) (1990) 2005-2010.

[27] A.L. Dendramis, E.W. Schwinn, R.P. Sperline, A surface-enhanced Raman scattering study of CTAB adsorption on copper, Surface Science 134 (3) (1983) 675-688.

[28] B.J. Ninness, A Molecular Investigation of Absorption onto Mineral Pigments., in: Chemical Engineering, Vol. Doctor of Philosophy, The University of Maine, Maine, 2001.

[29] S. Sun, R.L. Birke, J.R. Lombardi, Surface-Enchanced Raman Spectroscopy of Surfactant on Silver Electrodes, The Journal of Physical Chemistry 94 (5) (1990) 2005-2010.

[30] S.C. Howard, V.S.J. Craig, Adsorption of the Cationic Surfactant Cetyltrimethylammonium Bromide to Silica in the Presence of Sodium Salicylate: Surface Excess and Kinetics, Langmuir 25 (22) (2009) 13015-13024.

[31] C.T. Williams, Y. Yang, C.D. Bain, Total Internal Reflection Sum-Frequency Spectroscopy: A Strategy for Studying Molecular Adsorption on Metal Surfaces, Langmuir 16 (5) (2000) 2343-2350.

[32] J. Goworek, A. Kierys, W. Gac, A. Borówka, R. Kusak, Thermal degradation of CTAB in as-synthesized MCM-41, Journal of Thermal Analysis and Calorimetry 96 (2) (2009) 375-382.

[33] S.A. Wald, C.C. Winding, Differential thermal analysis using high frequency dielectric heating I. Theory and equipment, Polymer Engineering & Science 11 (1) (1971) 57-63.

[34] F.M. Etzler, J.J. Conners, A DSC/TGA method for determination of the heat of vaporization, Thermochimica Acta 189 (2) (1991) 185-192.

[35] M.A. Osman, U.W. Suter, Surface Treatment of Calcite with Fatty Acids: Structure and Properties of the Organic Monolayer, Chemistry of Materials 14 (10) (2002) 4408-4415.

[36] A. Swami, A. Kumar, M. Sastry, Formation of Water-Dispersible Gold Nanoparticles Using a Technique Based on Surface-Bound Interdigitated Bilayers, Langmuir 19 (4) (2003) 1168-1172.

[37] B. Wang, M. Zhou, Z. Rozynek, J.O. Fossum, Electrorheological properties of organically modified nanolayered laponite: influence of intercalation, adsorption and wettability, Journal of Materials Chemistry 19 (13) (2009) 1816-1828.

[38] W.P. De Klerk, Thermal Analysis of some propellants and Explosives with DSC and TG/DTA, in, 1996.

[39] M.J. Blandamer, P.M. Cullis, L.G. Soldi, K. Chowdoji Rao, M.C.S. Subha, Effects of added dotab on the<i>cmc</i> and enthalpy of micelle formation at 298.2 K for CTAB(aq), Journal of Thermal Analysis and Calorimetry 46 (6) (1996) 1583-1588.

[40] S.P. Stodghill, A.E. Smith, J.H. O'Haver, Thermodynamics of Micellization and Adsorption of Three Alkyltrimethylammonium Bromides Using Isothermal Titration Calorimetry, Langmuir 20 (26) (2004) 11387-11392.

[41] S. Paria, K.C. Khilar, A review on experimental studies of surfactant adsorption at the hydrophilic solid-water interface, Advances in Colloid and Interface Science 110 (3) (2004) 75-95.

[42] K.P. Sharma, V.K. Aswal, G. Kumaraswamy, Adsorption of Nonionic Surfactant on Silica Nanoparticles: Structure and Resultant Interparticle Interactions, The Journal of Physical Chemistry B 114 (34) (2010) 10986-10994.

[43] C. Wu, Laser Light Scattering Determination of the Surfactant Interface Thickness of Spherical Polystyrene Microlatices, Macromolecules 27 (24) (1994) 7099-7102.

[44] F. Zhao, Y.-K. Du, J.-K. Xu, S.-F. Liu, Determination of surfactant molecular volume by atomic force microscopy, Colloid Journal 68 (6) (2006) 784-787.

[45] A. Gurses, M. Yalcin, M. Sozbilir, C. Dogar, The investigation of adsorption thermodynamics and mechanism of a cationic surfactant, CTAB, onto powdered active carbon, Fuel Processing Technology 81 (1) (2003) 57-66.

[46] Z. Bu-Yao, G. Yu-Jun, W. Hong-Jian, Z. Guo-Xi, An Investigation on the Micelle-Catalytic Hydrolysis and Ammonolysis of Carboxylic Acid Esters, Acta Phys. -Chim. Sin. 12(02) (02) (1996) 109-113.

[47] X. Guo, Y. Deng, D. Gu, R. Che, D. Zhao, Synthesis and microwave absorption of uniform hematite nanoparticles and their core-shell mesoporous silica nanocomposites, Journal of Materials Chemistry 19 (37) (2009) 6706-6712.

[48] W. Zhao, M. Lang, Y. Li, L. Li, J. Shi, Fabrication of uniform hollow mesoporous silica spheres and ellipsoids of tunable size through a facile hard-templating route, Journal of Materials Chemistry *19* (18) (2009) 2778-2783.

[49] N.I. Ivanova, Adsorption of a surfactant mixture at the surface of calcium carbonate from aqueous solutions, Colloid Journal 62 (1) (2000) 56-60.

CHAPTER 4

Supporting Information

INITIAL INVESTIFATION ON THE PRECIPITATE SAMPLE FOR THE ADSORPTION OF CETYLTRIMETHYLAMMONIUM BROMIDE ONTO CALCIUM CARBONATE NANO-CUBE PARTICLES UNDER ALKALINE-AQUEOUS SOLUTION

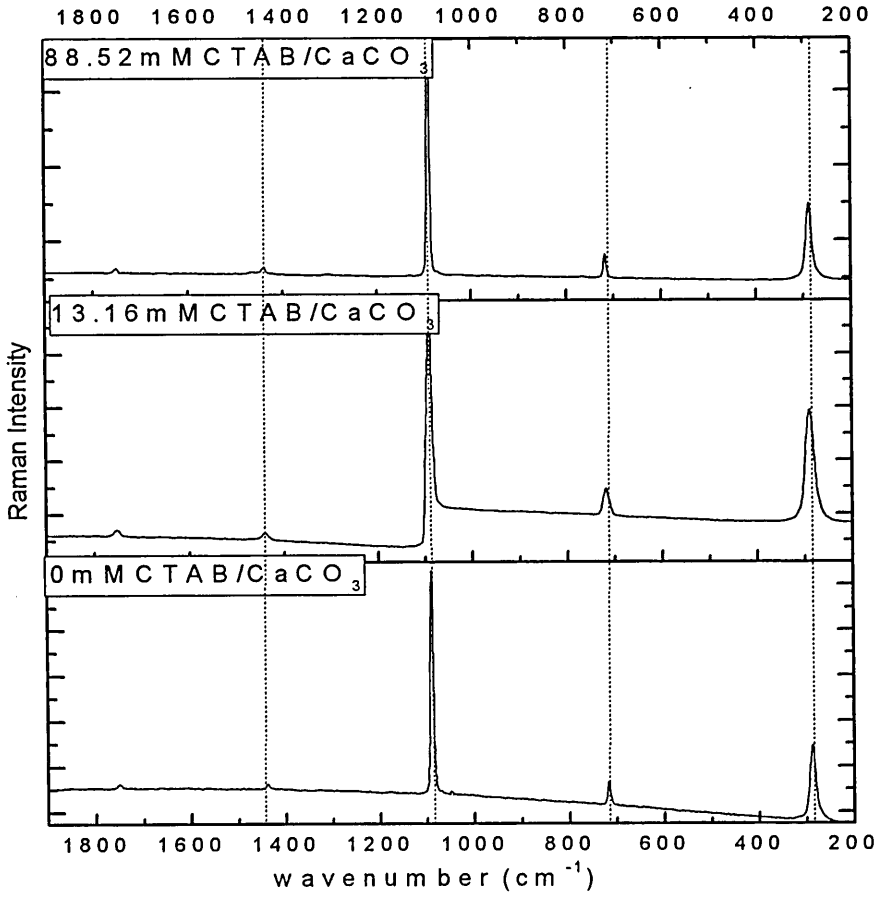

Figure 4.S 1 The Raman spectra (1800 – 200 cm^{-}) of CTAB adsorbed on $CaCO_3$ nanoparticles from 0 mM CTAB-$CaCO_3$ (raw material), 13.16 mM CTAB-$CaCO_3$ and 88 mM CTAB-$CaCO_3$.

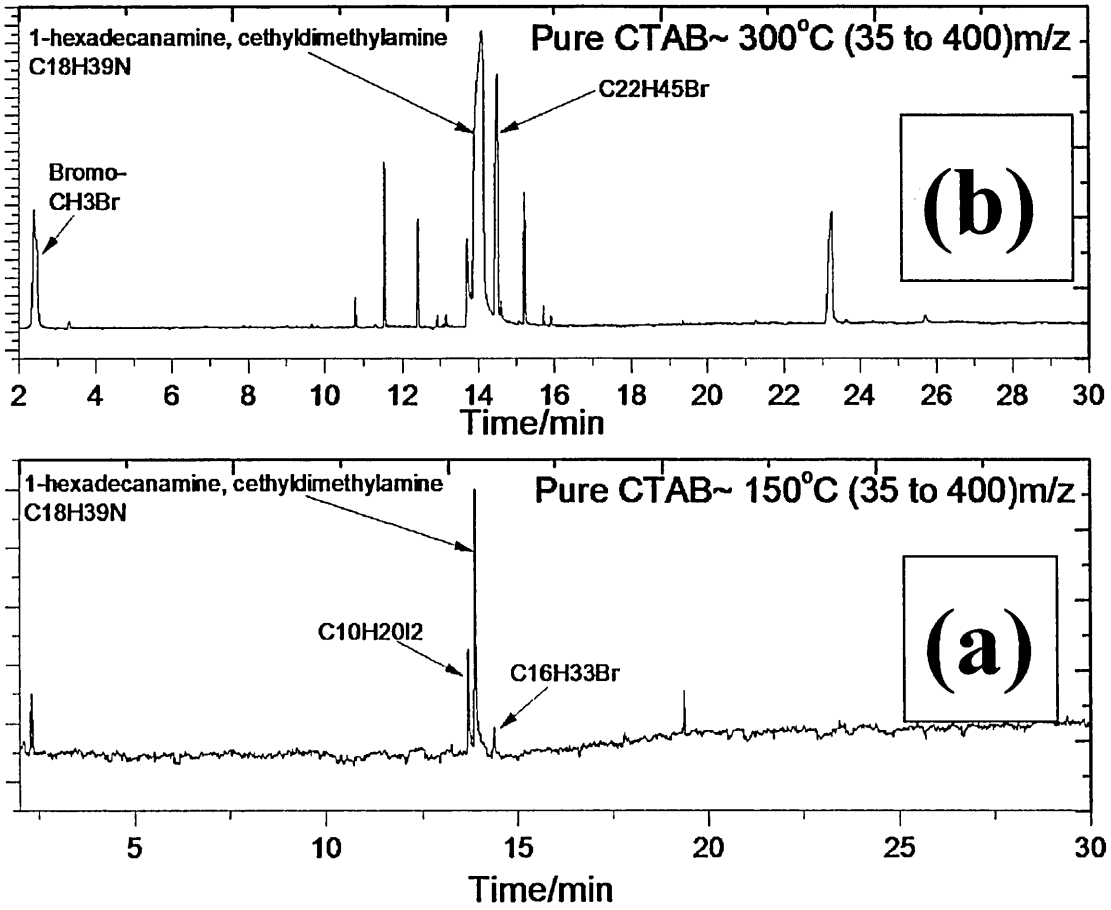

Figure 4.S 2 GC-MS analysis of pure CTAB powder degradation product; (a) 150°C and (b) 300°C

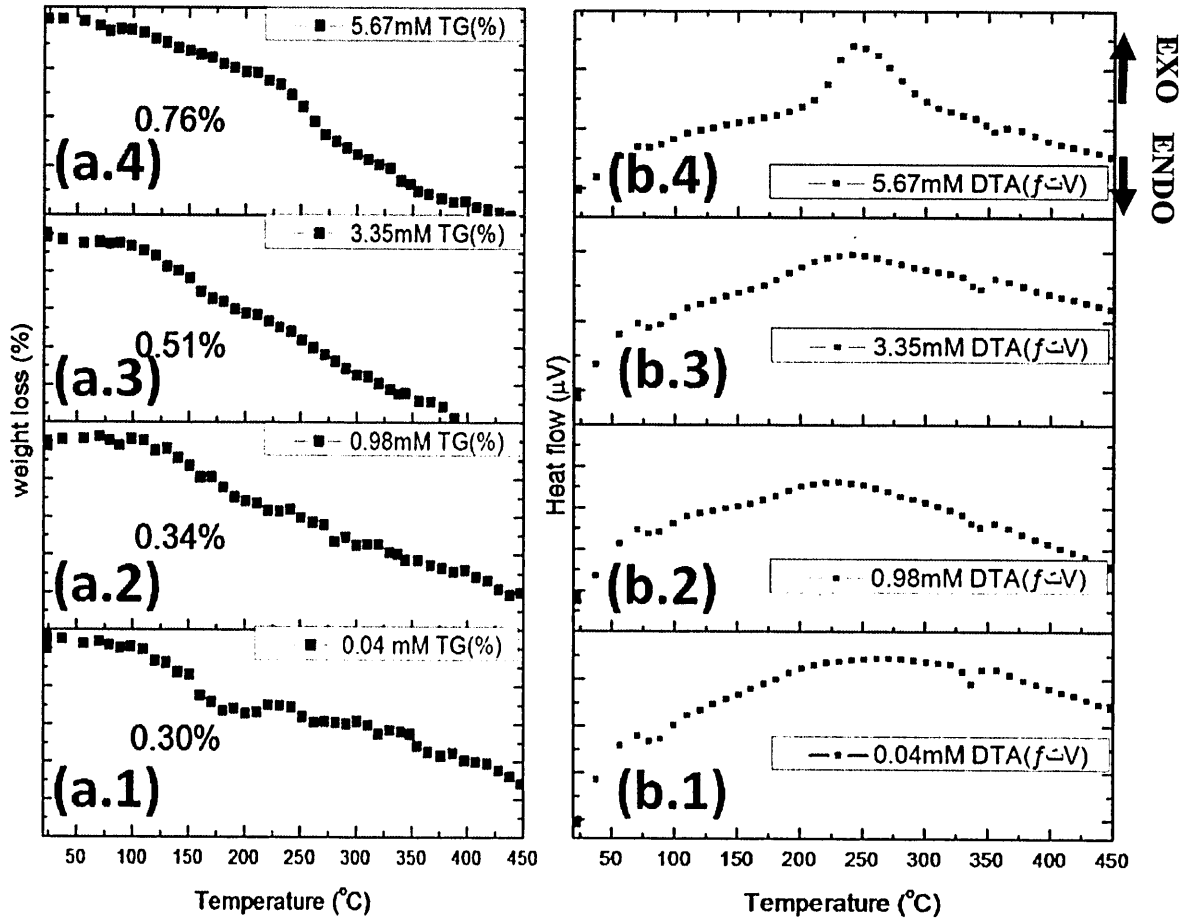

Figure 4.S 3 DTA (b) and TG (a) analysis at 25°C to 500°C CTAB adsorption at increasing concentration (mM) onto $CaCO_3$ nanoparticles under alkaline condition

Properties	Nanocube $CaCO_3$	5.67 mM CTAB/$CaCaCO_3$	35.31 mM CTAB/$CaCaCO_3$	88.52 mM CTAB/$CaCaCO_3$
Specific surface area BET (0.5 – 0.15) p/p_0	12.05	12.57	13.80	13.39

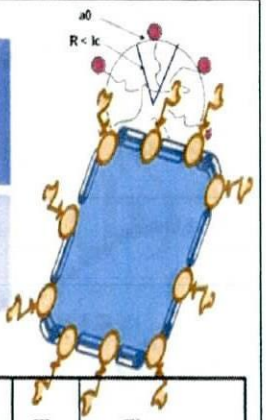

Theoretical calculation for the total weight of CTAB one layer monomer absorb covering the surface of $CaCO_3$ cubic nanoparticles (W_{TCTAB})

Assume parameters:

SSa = total specific surface area of the raw $CaCO_3$ nanoparticles = 12.05 m^2/g = $1.205 \times 10^{+19}$ nm^2/g

W_C = weight of the actual weight $CaCO_3$ nanoparticles = 3.32 g

Optimum Hydrophilic head area (a_0) range: (0.19 to 0.64) nm^2

Density of the calcite $CaCO_3$ (true density) ρ_T = 2.71 g/nm^3

MW_{CTAB} = molecular weight of CTAB = 364.45 g/mole

N_A = Avogadro's number = 6.023×10^{23}/mole

V_{actual} = Volume actual used = 0.02539L

Then total number of CTAB head area molecules attach to the surface of each $CaCO_3$ nanoparticles is

$N_{TCTAB/CaCO3/3.32} = (SSa / a_0)(W_C) = (1.205 \times 10^{+19}\ nm^2/g / 0.64\ nm^2)(3.32g)$

$N_{TCTAB/CaCO3/3.32} = 6.25 \times 10^{+19}$ ---------- (A)

Thus the weight of CTAB molecules (1 layer) covering each cubic $CaCO_3$ nanoparticles

$W_{total\ CTAB\ molecules/CaCO3} = (N_{TCTAB/CaCO3/3.32} \times MW_{CTAB})/N_A$

$W_{total\ CTAB\ molecules/CaCO3} = (6.25 \times 10^{+19} \times 364.45\ g/mole) / 6.023 \times 10^{23}/mole$

$W_{total\ CTAB\ molecules/CaCO3} = 0.0378\ g$ ---------- (B) ~ (1.14%)

milliMolar = [(0.0378 g)(1 mole/364.45)]/ 0.02539 L = 4.0 mM proximate cocn.

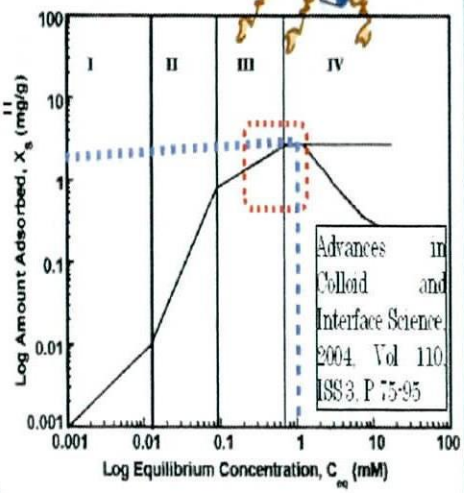

Fig. 5. Schematic presentation of typical four-regime adsorption isotherm [44].

Adsolubilization of Styrene and Isoprene

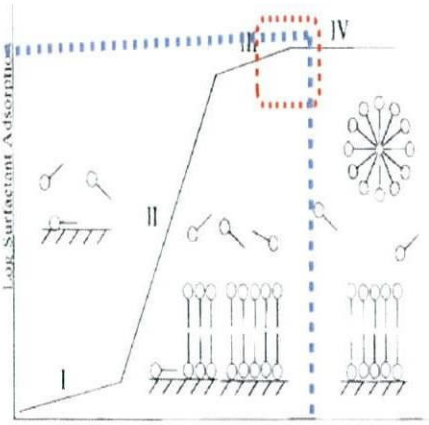

Figure 1. Typical adsorption isotherm of surfactants on solid oxide surfaces.

Figure 4.S 4 Theoretical calculation of full monolayer coverage of CTAB on $CaCO_3$ nanoparticles

CHAPTER 5

FACILE ROUTE IN FABRICATING STABLE AND COMPOSITE SHELL HOLLOW SILICATE NANOPARTICLES BY AMMONIA-HYDROTHERMAL PROCESS

CHAPTER 5

FACILE ROUTE IN FABRICATING STABLE AND COMPOSITE SHELL HOLLOW SILICTAE NANOPARTICLES BY TEMPLATED AMMONIA –HYDROTHERMAL PROCESS

5.1 Introduction

Inorganic nano-sized hollow silica particles have received more attention compared with other hollow particles because of intensive well-defined architectures. Most of hollow silica particles have low density, low toxicity, and high surface area with high chemical and thermal stability. This nano-size hollow silica particle can pave way for the applications in catalysis, controlled drug delivery and light filler material [1-5]. Various methods used in fabricating inorganic hollow particle namely have been reported such as (i) inorganic template directed synthesis [6-10] and (ii) emulsion synthesis [11]. In addition, a hollow inorganic composite core/shell particle has been made by templating routes, which make use of vesicles, acoustic cavitations, or electrically forced liquid jets [12-14]. Yet, it is still a challenge to develop environmentally friendly, simple, and versatile approaches to synthesize a hollow inorganic composite core/shell micro- and nanostructures that will greatly facilitate the future application of these hollow nano-materials in various fields. But, simpler methods for controlled preparation of hollow composite nano-materials would be more favored. Thus, our laboratory has an extensive research work undertaken into the synthesis of inorganic silica hollow nanoparticles over the past decade via template method. In this research work, novel amorphous nano-size hollow calcium-silicate hydrate particles have been synthesized using ammonia-hydrothermal template method.

As mentioned, we describe a novel size, low temperature hydrothermal reaction (less than 150^0C) for synthesis of hollow calcia-silicate nanoparticles using $CaCO_3$ as templates. Calcium-silicate hydrate ($Ca(OH)_2$-SiO_2) composite shells encapsulate into the core nanoparticles was obtained by ammonia-hydrothermal aging for 10 d with agitation at 120 °C wherein the size and shape of the hollow particles can be controlled by the dimensions of the core nanoparticles.

This chapter investigated the physicochemical properties such as thermal property, crystallinity and morphology of the synthesized unique hollow $Ca(OH)_2$-SiO_2 nanoparticles. Furthermore, the calcium-silicate hydrate hollow nanoparticles have a potential for future applications such as for cement industry and biomaterials.

5.2 Starting materials and schematic outline

5.2.1 Materials

Nano-cube 60 Calcium carbonate ($CaCO_3$, RMHA) (Nittetsu Kogyo) was used as core particles and a source of calcia during hydrothermal process. Tetraethoxysilane (Wako pure chemical) was used as precursor of silica shell. Ammonia water (28% Wako pure chemical) used as catalyst and Ethanol (Wako pure chemical) used as a solvent for the hydrothermal sol gel template reaction.

5.2.2 Synthesis of hollow calcia-silicate nanoparticles

New nano-sized hollow calcium-silicate hydrate particles were first synthesized based on the previous method done by our laboratory (CRL, NIT) using calcium carbonate as template [2]. Calcium carbonate ($CaCO_3$), ethanol (EtOH), tetraethoxysilane (TEOS) and ammonium aqueous solution (H_2O:NH_3) were mixed and stirred for 2 h at ambient temperature with the molar ratio of 7.3:58.9:1:7.8:3.4 ($CaCO_3$:

EtOH: TEOS: H_2O:NH_3), a core-shell calcium carbonate / silica particles was prepared. In obtaining hollow calcium-silicate hydrate nanoparticles, after 2 h continuous stirring, the white gel solution was divided into three parts, one part was for control (no hydrothermal) (HS0dAH0) and the other two parts were 90 °C (HS10d90H1) and 120 °C (CS10d120H2) hydrothermally treated solutions. The two parts white gel solution was separately placed in a 50 mL capacity autoclaveble Teflon-lined stainless steel with estimated maximum pressure of 50 kg/cm^2, which was heated to 90 °C and 120 °C for 10 d. The synthesized product were filtered and washed several times (4X or until becomes neutral) by ethanol, then dried in a vacuum oven to 90 °C for 5 h. In removing the calcium carbonate core, acid treatment (3.0 mol/L, HCl) was done for 8 h stirring. After then, filtered and washed several times (4X or until becomes neutral) with distilled water. Finally, vacuum dried the obtained sample to 90 °C for 1 d, hollow calcium-silicate hydrate nano-size particle was obtained. The process flow in synthesizing hollow calcium-silica hydrate nanoparticles is shown in Figure 5.1

5.2.3 Physico-chemical characterization

The product were characterized by X-ray Diffraction (XRD, Model RINT 1100, Rigaku) with Cu Kα radiation (λ= 1.54056 Å), at a scanning rate of 0.02 °/ s (5 ° to 60 °, 2θ) with an operating voltage of 40 kV and emission current 30 mA. The thermal property of the sample was investigated using the Thermogravimetry (TG, TG-8120, Rigaku, Japan) under oxygen atmosphere. The heating rate of the temperature increase at 10 °C/min with temperature ranged from (22 to 1000) °C. Morphology and microstructure of hollow particles were examined using scanning electron microscopy (SEM; JSM-7000F, JEOL). The specific surface area and cavity (pore) size

distribution of the sample were determine by Barrett-Joyner-Halenda (BJH) method via the automatic surface area analyzer (BELSORP-max) with Nitrogen gas adsorption and desorption isotherm recorded at 77K.

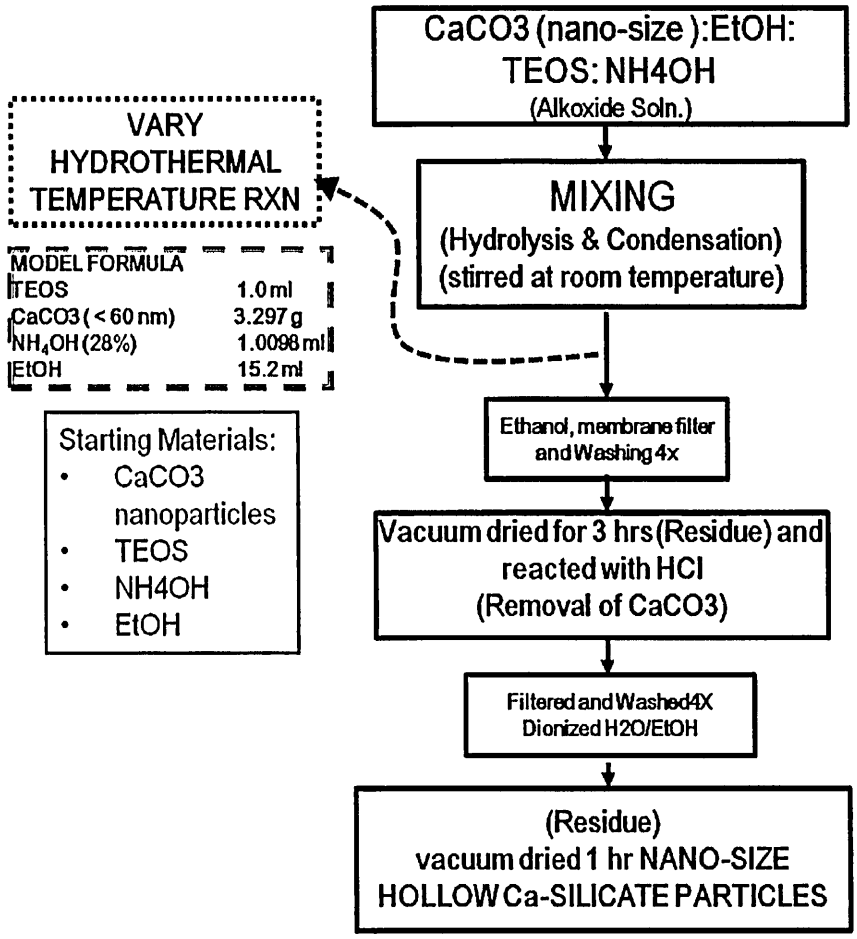

Figure 5. 1 Process flow for the synthesis of nano-size hollow calcium-silicate hydrate particles using $CaCO_3$ nanoparticles as template core.

5.3 Results and discussions

5.3.1 Structure analysis by X-ray Diffraction pattern (XRD)

XRD patterns of non-coated calcium carbonate nanoparticles (RMHA, Figure 5.2a), calcium carbonate nanoparticles coated with silica synthesized at ambient

temperature for 2 h (HSOdAH0, Figure 5.2b), and hydrothermally treated nanoparticles calcium carbonate coated with silica at 90 °C (HS10d90H1, Figure 5.2c) and 120 °C for 10 d (CS10d120H2, Figure 5.2d) were compared in Figure 5.2. The non-hydrothermal coating sample (HSOdAH0, Figure 5.2b) showed a diffraction angle identified as calcite (core nanoparticles $CaCO_3$) a cubic unit cell. This shows that the sharp reflection peaks indicate a crystalline structure of the cubic $CaCO_3$ which signify that the amorphous silica hypothetically coated in the core nanoparticles.

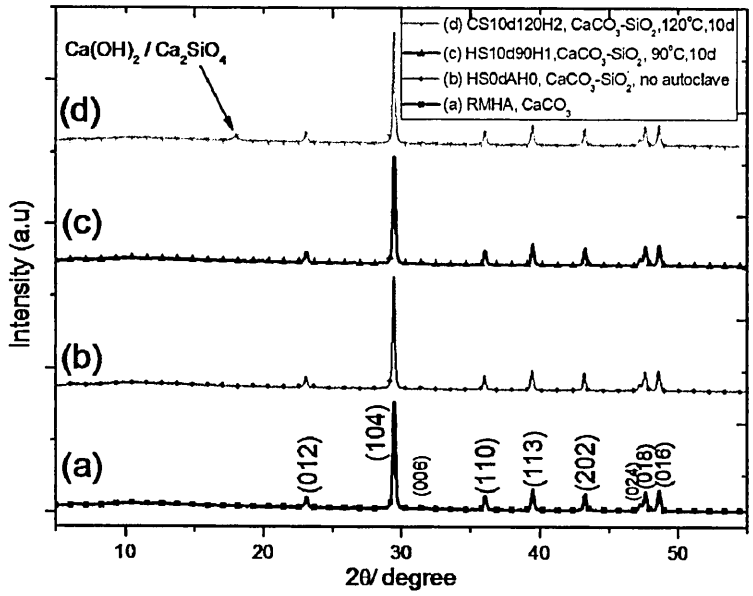

Figure 5. 2 XRD pattern measured for (a) raw cubic calcite ($CaCO_3$) [RMHA]; (b) silica coated $CaCO_3$ nanoparticles without acid treatment [HS0dAH0]; (c) silica coated $CaCO_3$ nanoparticles hydrothermally treated for 10 d agitation at 90 °C [HS10d90H1] and (d) 120 °C without acid treatment [CS10d120H2].

While the sample CS10d10H2 (hydrothermally treated, Figure 5.2d), formed an additional sharp peak at 18.1 (2θ) aside from the peaks of the cubic raw $CaCO_3$ core nanoparticles. The additional peaks corresponds to $Ca(OH)_2$ (Portlandite) [15] and

Ca_2SiO_4 (Larnite) [15] after 10 d agitation in 120 °C (Figure 5.2d) except for 90 °C no reflection peak form at 18.1 (2θ) after 10 d agitation (HS10d90H1, Figure 5.2c).

In order to confirm that the deposition of $Ca(OH)_2$ and formation of Ca_2SiO_4 were indeed in the core-shell of amorphous silicate structure after ammonia-hydrothermal treatment at 120 °C for 10 d; acid dissolution was done for all the experimental samples. As anticipated, after acid treatment for 8 h stirred, filtered , washed 4X with distilled water and dried, reflection peak at 18.1 (2θ) still exist for the sample CS10d120H2 (Figure 2c). While no visual peaks (no other crystalline phases) was observed for sample HS0dAH0 (Figure 2a) and HS10d90H1 (Figure 5.3b)

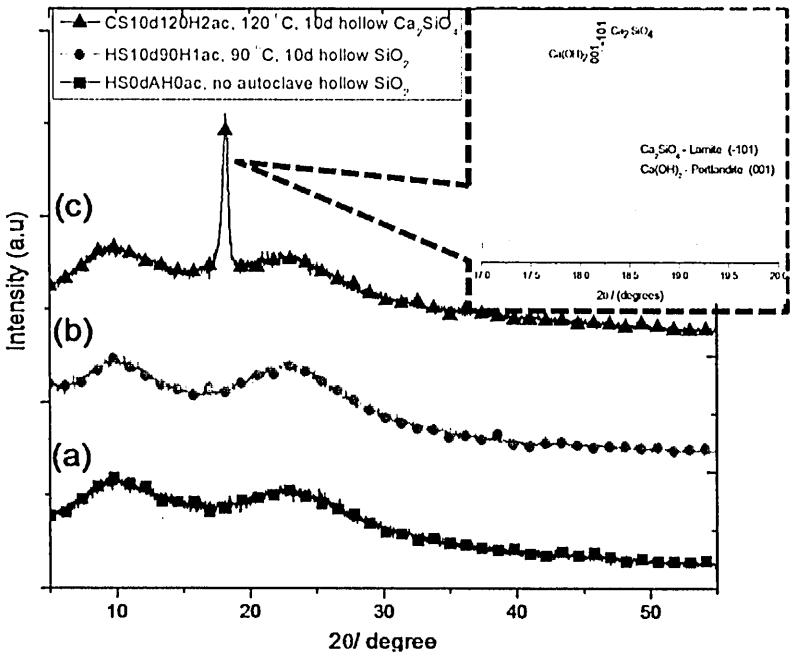

Figure 5. 3 XRD pattern measured for (a) hollow silica nanoparticles after acid treatment [HS0dAH0ac]; (b) hollow silica nanoparticles process at 90 °C after acid treatment [HS10d90H1ac] and (c) hollow calcium-silicate hydrate nanoparticles process at 120 °C after acid treatment [CS10d120H2ac]. Inset image showing the reflection pattern of $Ca(OH)_2$ [Portlandite , (001)] and Ca_2SiO_4 [Larnite, (-101)].

.For the sample CS10d120H2 (Figure 5.3c), a formation of hollow amorphous calcia-silica nanoparticles, as shown in the inset, enlarge XRD pattern of sample CS10d120H2 was shown. From the peaks, it was clearly shown that the crystalline peaks of $Ca(OH)_2$ (001) and Ca_2SiO_4 ($\bar{1}01$) which corresponds to Portlandite (15a) and Larnite (15b) respectively were formed after ammonia-hydrothermally agitated at 120 °C for 10 d. For enlarge XRD patterns of calcium silicate hydrate see Figure 5.S.3.

5.3.2 Morphological observations

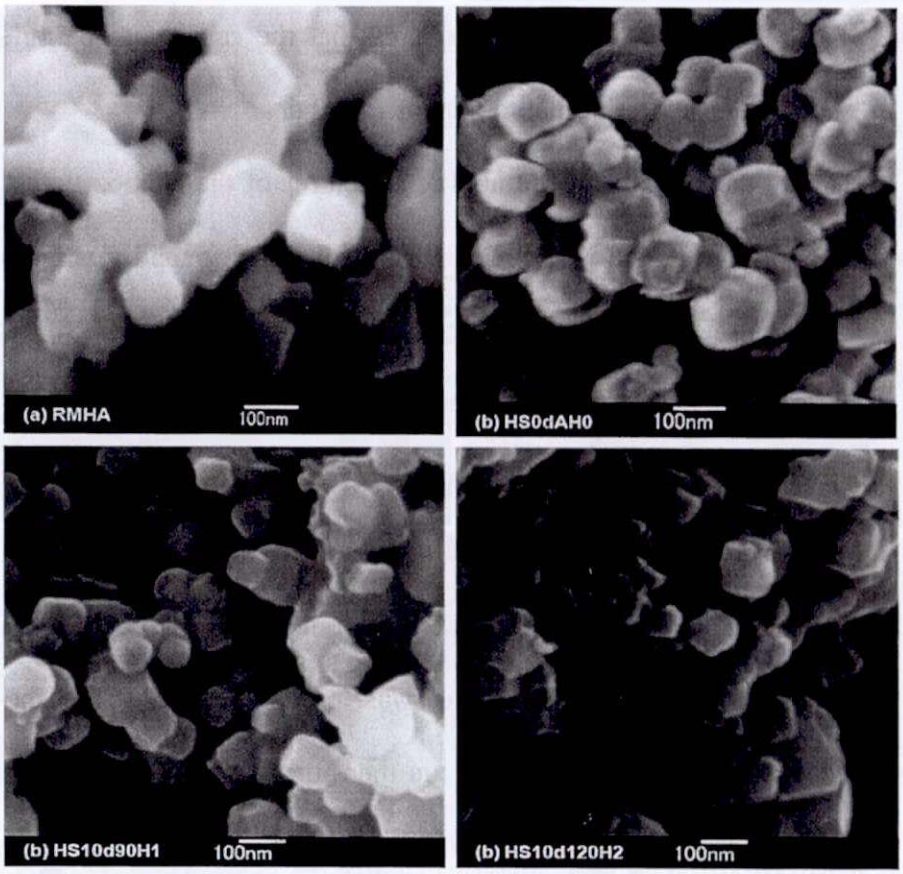

Figure 5. 4 SEM images : (a) $CaCO_3$ raw (cubic) [RMHA] , (b) $CaCO_3$ coated with SiO_2 without hydrothermal [HS0dAH0] , (c) $CaCO_3$ coated with SiO_2 by hydrothermal at 90 °C for 10 d [HS10d90H1], (d) $CaCO_3$ coated with SiO_2 by hydrothermal at 120 °C for 10 d [CS10d120H2].

The scanning electron microscopy (SEM) was further conducted. In Figure 5.4 and 5.5(ab,c,d) were the surface observation of the synthesized hydrothermally template samples before and after acid treatment respectively. As shown in Figure 5.4a, (before acid treatment) reveal that the samples (HS10d90H1 and CS10d120H2) hydrothermally treated at (90 and 120) °C for 10 d consist of cubic smooth shape surface (Figure 5.4c HS10d90H1 and Figure 5.4d CS10d120H1) has the same shape from the original raw materials cubic $CaCO_3$ (Figure 5.4a RMHA) and sample synthesized at ambient temperature (Figure 5.4b HS0dAH0). It indicated that the cubic core particles (cubic $CaCO_3$) were stable after hydrothermal treatment for 10 d.

To validate the stability of the hollow structures of the nanoparticles obtained by this method, the synthesized nanoparticles were subjected to acid treatment for 8 h, filtered and dried. As seen in Figure 5.5(b,c,d), a hollow structure with (30 to 100) nm nanoparticles was clearly observed for the samples synthesized in ambient and hydrothermal treatment. The hollow nanoparticles have thin walls whose thickness appears to be uniform around the shell and smooth outer surface as shown in Figure 5.5b, 5.5c and 5.5d. While in TEM images as shown in Figure 5.5e, 5.5f and 5.5g, the structural stability of the hollow particles was established. Clearly, shown that amorphous silicate shell became more firm and then formed a calcium-silicate hydrate shell upon increasing hydrothermal temperature at 10 d aging. Thereby appeared stable cubic hollow hybrid silicate nanoparticles were accomplished after acid treatment which can be observed in Figure 5.5(f & g). These indicates that the formation and deposition of $Ca(OH)_2$ into the amorphous silicate sheet was likely in the surface of cubic $CaCO_3$ after hydrothermally agitated at 120 °C for 10 d.

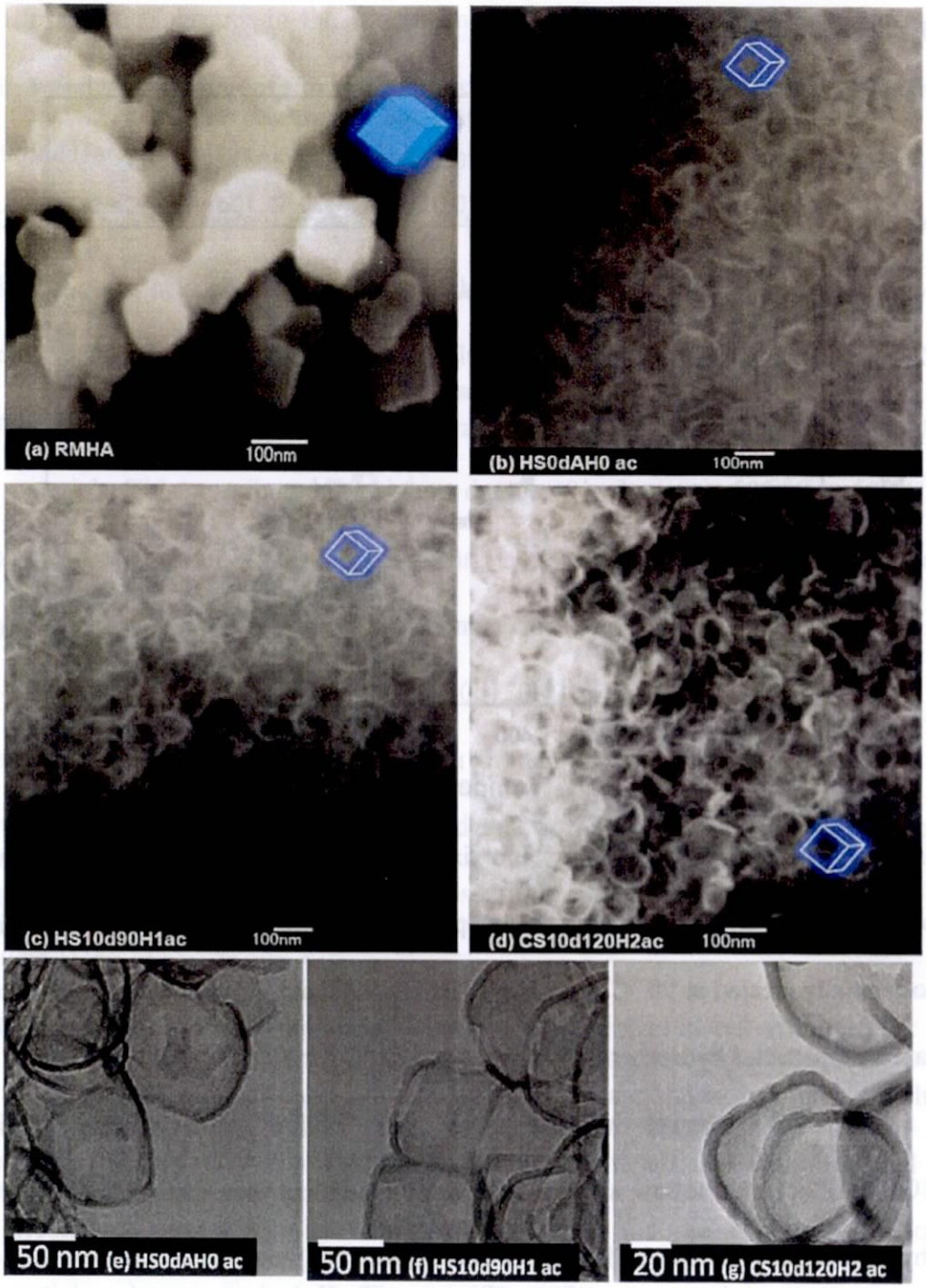

Figure 5. 5 SEM and TEM images: (a) [RMHA] $CaCO_3$ raw (cubic); Acid treated samples (b & e) [HS0dAH0ac] nano-sized hollow SiO_2 without hydrothermal, (c & f) [HS10d90H1ac] nano-size hollow SiO_2 by hydrothermal at 90 °C for 10 d (d & g) [CS10d120H2ac] nano-size hollow $Ca(OH)_2$-SiO_2 with hydrothermal at 120 °C for 10d.

5.3.3 Thermo analytical analyses

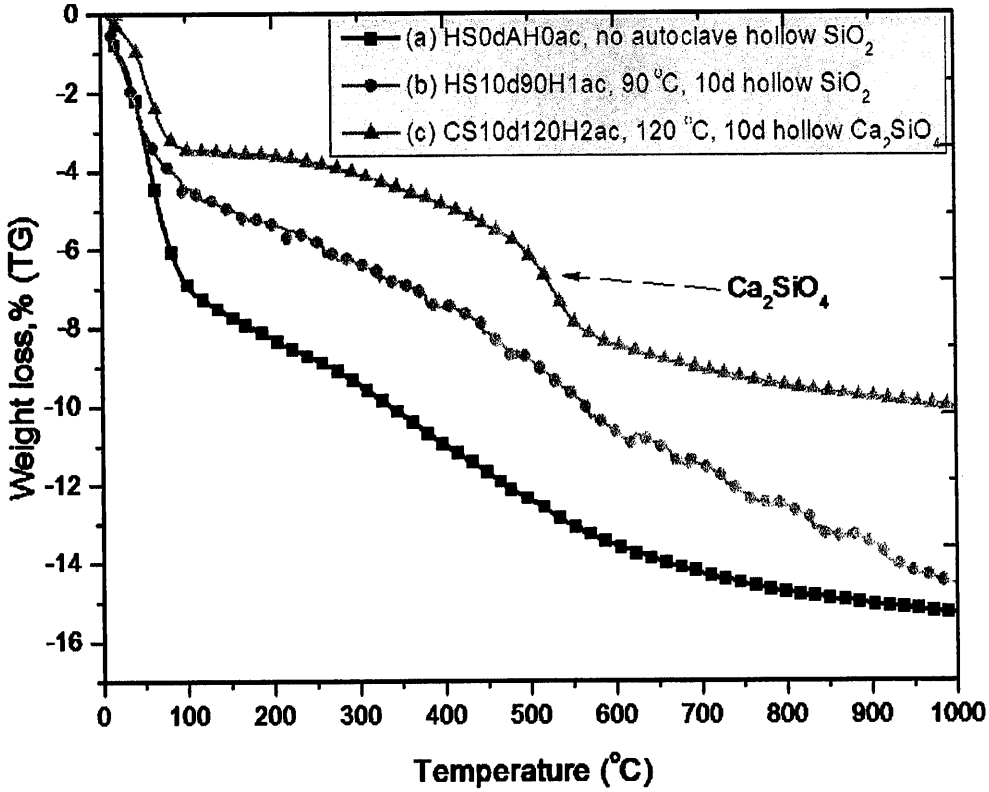

Figure 5. 6 TG thermogram of the nano size hollow particles after acid treatment (a) hollow particles synthesized at ambient temperature [HS0dAH0ac], (b) hollow particles hydrothermally treated at 90 °C for 10days [HS10d90H1ac], (c) hollow calcium-silicate hydrate nanoparticles hydrothermally treated at 120 °C for 10 d [CS10d120H2ac].

The TGA curves of the nano size hollow calcia-silicate particles (CS10d120H2ac), the hollow silica synthesized at ambient temperature (HS0dAH0ac) and hydrothermally treated hollow silica (HS10d90H1ac) nanoparticles were shown in Figure 5.6. In general, three significant temperature regions as far weight loss steps (TGA) and then the samples experiences no further weight loss. Region I (below 150 °C) as the first weight loss is due to the bound water removal [16] or desorption of unattached molecular water. While in region II (200 to 500) °C is mainly attributed

some loss of OH^- groups in the silanol groups in the frameworks which attribute to slight weight loss [17] of the all the experimental samples namely HS0dAH0ac, HS10d90H1ac and CS10d120H2ac. But the exceptional weight loss is in region III (500 to 600) °C which apparently visible only in CS10d120H2ac hollow sample, were due to the formation of new phases contained in the core shell from the amorphous nano size hollow calcium-silicate hydrate. The results collaborated with the analysis of XRD wherein the presence of deposited $Ca(OH)_2$ in the amorphous silicate which formed a new materials. This contributed the highest degree of hydration at 500 °C to 600°C [18] which clearly shown in Figure 5.6. This was also confirmed during 29 Si NMR spectra analysis wherein the C-S-H peaks have chemical shifts approximately around -78.9 ppm and -87.6 ppm [19-21] at the sample CS10d120H2ac as shown in Figure 5.S.4. This affirms that $Ca(OH)_2$ can be deposited in the shell of amorphous silica sheet after hydrothermal treatment at 120 °C for 10 d that attributed to the presence of drop of weight loss which is not visibly present for the samples HS0dAH0ac and HS10d90H1ac.

5.3.4 N_2 adsorption isotherms and Cavity space (pore size) distributions

The nitrogen adsorption isotherms of samples are shown in Figure 5.7. It can be seen BET surface area of the synthesized hollow nanoparticles were measured after acid treatment. The absorption isotherms at 77 K for the experimental hollow nanoparticles show a typical II. The specific surface area and average space pore diameters are (298.76, 227.13 and 136.45) m^2/g and (29.50 to 46.13) nm for a normal nano-size hollow silica particles (HS0dAH0ac), hydrothermally treated hollow nanoparticles HS10d90H1ac and CS10d120H2ac. The lower surface area of hollow

calcium-silicate hydrate sample (CS10d120H2ac) could be due to the thickening of framework (silanol groups) walls [22] that accelerated the deposition of $Ca(OH)_2$ into the amorphous silica shell.

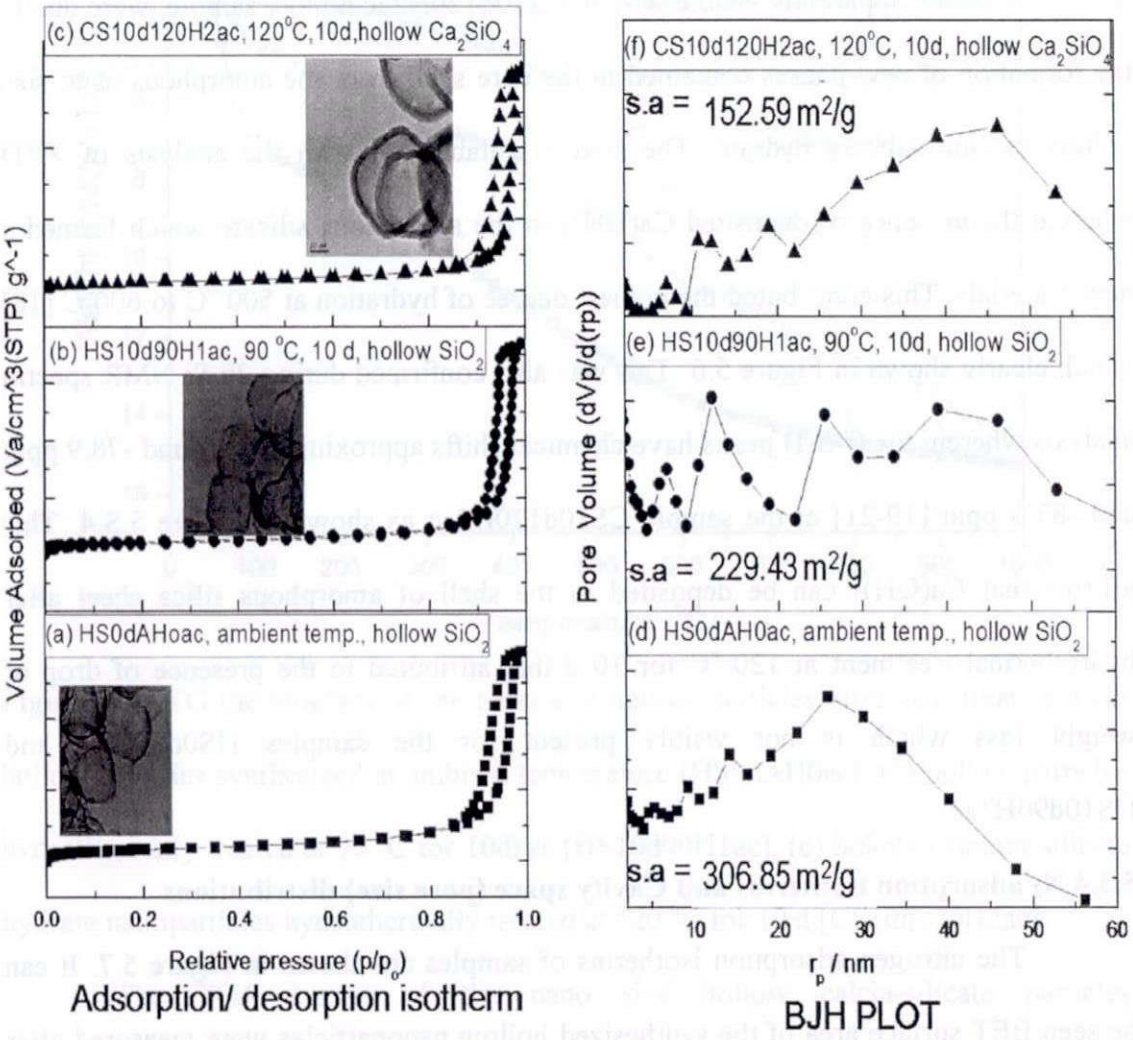

Figure 5. 7 Nitrogen adsorption-desorption isotherms (a to c) and BJH differential pore size distribution (d to f) of hollow particles synthesized at ambient temperature (HS0dAH0ac), hollow particles hydrothermally treated at 90 °C for 10 d (HS10d90H1ac) and hollow calcium-silicate nano particles hydrothermally treated at 120 °C for 10 d (CS10d120H2ac). (inset images are the TEM images of the respective hollow particles)

This enhances the structure stability of the silica hollow spheres as shown in SEM images (Figure 5.5) wherein cubical shape still exist with no major apparent change of the hollow samples, suggesting that the synthesize hollow samples (calcium-silicate hydrate) have a higher hydrothermal stability.

5.3.5 Mechanism of the hollow calcium-silicate hydrate nanoparticles

From the results obtained, possible mechanism for the formation of the hollow calcia-silicate nanoparticles was described in the Figure 5.8.In the coating process, TEOS was added to the ammonia-contained $CaCO_3$ nanoparticles for sol-gel reaction. Under this condition, silica formed as the shell on the core particles via ammonia-catalyzed hydrolysis and condensation of TEOS [2, 7, 23]. Note that the coating process was conducted at room temperature. Then during hydrothermal treatment, increasing the temperature with pressure accelerates the polymerization and resulted in the dissolution of the silica framework [22]. The effects of hydrothermal treatment on silicate structure coreshell were evident especially at the temperature 120 °C as shown Figure 5.2. It is believed that there were two main reasons for this: (i) the silicate framework condenses and (ii) undergoes reconstruction under hydrothermal conditions [24].

This implies that a rearrangement of silica framework was taken place at high temperature during hydrothermal template synthesis of the hollow nanoparticles. This led to the range order of pore increases that will help $Ca(OH)_2$ deposited in the amorphous silica core shell.

In addition, the solubility of $CaCO_3$ by hydrolysis with increasing temperature was accelerated under hydrothermal conditions. Then Ca^{2-} and OH^- ions form $Ca(OH)_2$

may occur on the surface of $CaCO_3$ powder particles with increasing temperature and pressure. The large number of active hydroxyl groups with the presence of Ca^{2-} ions on the surface of the nano-size CaCO3 can give rise to strong interaction between amorphous hollow silicate core sheet nanostructure [24, 25]. This interaction, $Ca(OH)_2$ formed on the surface and deposited to the amorphous silica sheet due to the rearrangement of silica framework during hydrothermal treatment [26]. The existence of $Ca(OH)_2$ and Ca_2SiO_4 oxides in the amorphous phase of silica was due to the hydrothermal. Hence, a new nano size hollow calcium-silicate hydrate particle was formed as shown in Figure 5.5d.

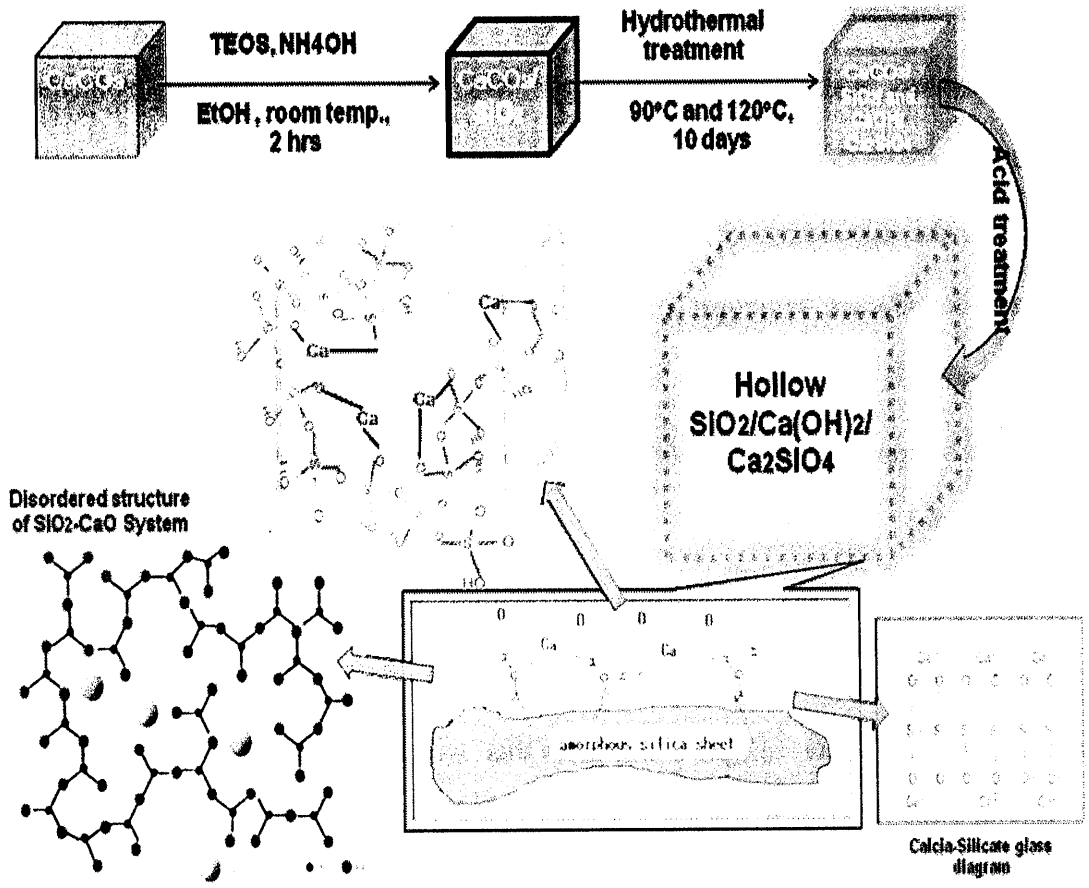

Figure 5. 8 Schematic Illustration for the formation of Hollow calcium-silicate hydrate Nanoparticles

5.4 Conclusion

In this chapter, a facile and novel size for the formation of calcium-silicate hydrate hollow nanoparticles based on ammonia-hydrothermally $CaCO_3$ template sol gel process was done. The nanoparticles ($CaCO_3$) were dispersed in ethanol with the addition of TEOS and ammonia hydroxide for at least 2 h. Then silica shell were coated on the $CaCO_3$ nano-size particles via ammonia catalyzed hydrolysis and condensation of TEOS. The $CaCO_3$ coated with silica nanoparticles solution were subjected to hydrothermal sol gel reaction at (90 and 120) °C for 10 d. Then acid treatment was done to form hollow nanoparticles. As expected, hydrothermally stable cubic hollow shape and unique nano-sized hollow calcium-silicate hydrate particles were produced after ammonia-hydrothermally treated at 120 °C for 10 d. This nano-size hollow calcium-silicate hydrate particle has a good potential used for nano-cement (science) application and as a good source for a bioactive material. On the basis of this technique, other inorganic hollow particles with various shell compositions (e.g., Na_2O, TiO_2, Al_2O_3, B_2O_3, and etc.), a hollow nano glass-ceramic such as soda-lime, borosilicate hollow nanoparticles or different cavity sizes (e.g., 100 nm to micrometers) could be produced.

References

[1] X.-H. Li, D.-H. Zhang, J.-S. Chen, Synthesis of Amphiphilic Superparamagnetic Ferrite/Block Copolymer Hollow Supmicrosheres, Journal of American Chemical Society 128 (2006) 8382-8383.

[2] M. Fuji, C. Takai, Y. Tarutani, T. Takei, M. Takahashi, Surface properties of nanosize hollow silica particles on the molecular level, Advanced Powder Technology 18 (2007) 81-91.

[3] S. Hyuk Im, U. Jeong, Y. Xia, Polymer hollow particles with controllable holes in their surfaces, Nature Materials 4 (2005) 671-675.

[4] H. Zou, S. Wu, J. Shen, Polymer/Silica nanocomposite: preparation, characterization, properties and application, Chemical Review 108 (9) (2008) 3893-3957.

[5] A.P.R. Johnston, B.J. Battersby, G.A. Lawrie, M. Trau, Porous functionalized silica particles: a potential platform for biomolecular screeening, Chemical Communication (2005) 848-850.

[6] F. Caruso, R.A. Caruso, H. Mohwald, Nanoengineering of inorganic and hybrid hollow spheres by colloidal templating, Science 282 (2008) 1111-1114.

[7] H. Watanabe, M. FUJI, M. TAKAHASHI, Synthesis, characterization and application of nano-sized hollow silica particles, in: Proceeding 9th Ceramic Materials and Components for Energy and Environmental Appliation and Lazer Ceramics Symposium Conference, China, 2008, pp. 145-150.

[8] Y.S. Han, G. Hadiko, M. FUJI, M. Takahashi, A novel approach to synthesize hollow calcium carbonate particles, Chemistry letters 34 (2) (2005) 152-153.

[9] S.-J. Ding, C.-L. Zhang, M. Yang, X.-Z. Qu, Y.-F. Lu, Z.-Z. Yang, Template synthesis of composite hollow spheres using sulfonated polystyrene hollow spheres, Polymer 47 (2006) 8360-8366.

[10] J.H. Bang, K.S. Suslick, Sonochemical synthesis of nanosized hollow hematite, Journal of American Chemical Society 129 (2007) 2242-2243.

[11] S. Vaucher, M. Li, S. Mann, Synthesis of Prussian blue nanoparticles and nanocrystal superlattices in reverse microemulsion, Angew. Chem. Int. Ed. 39 (10) (2000) 1793-1796.

[12] S.S. Kim, W. Zhang, T.J. Pinnavaia, Ultrastable mesostructured silica vesicles, Science 282 (1998) 1302-1304.

[13] J. Shah, T.J. Pinnavaia, Thiol-functionalized mesostructured silica vesicles, Chemical Communication (2005) 1598-1600.

[14] C. Yu, B. Tian, J. Fan, G.D. Stucky, D. Zhao, Synthesis of Siliceous Hollow Spheres with Ultra Large Mesopore Wall Structures by Reverse Emulsion Templating, Chemistry Letters 31 (2002) 62-63.

[15] PCPDFWIN, JCPDS-International Center for diffraction data, in: (a) (04-0733) Portlandite

(b) (83-0461) Larnite, 1998.

[16] S.C. Mojumdar, L. Raki, Preparation, thermal, spectral and microscopic studies of calcium silicate hydrate-poly(acrylic acid) nanocomposite materials, Journal of Thermal Analysis and Calorimetry 85 (1) (2006) 99-105.

[17] J.-A. Kim, J.-K. Suh, S.-Y. Jeong, J.-M. Lee, S.-K. Ryu, Hydration reaction in synthesis of crystalline-layered sodium silicate, journal of Industrial and Engineering Chemistry 6 (4) (2000) 219-225.

[18] E.T. Stepkowska, Z. Sulek, J.L. Perez-Rodriguez, A. Justo, C. Maqueda, Thermal and microstructural studies on mud with additives, Journal of Thermal Analysis 37 (1991) 1497-1511.

[19] J. Schneider, M.A. Cincotto, H. Panepucci, 29Si and 27Al high-resolution NMR characterization of calcium silicate hydrate phases in activated blast-furnace slag pastes, Cement and Concrete Research 31 (7) (2001) 993-1001.

[20] J.J. Beaudoin, L. Raki, R. Alizadeh, A 29Si MAS NMR study of modified C–S–H nanostructures, Cement and Concrete Composites 31 (8) (2009) 585-590.

[21] R. I.G, The calcium silicate hydrates, Cement and Concrete Research 38 (2) (2008) 137-158.

[22] J.-H. Sun, M.-O. Coppens, A hydrothermal post-synthesis route for the preparation of high quality MCM-48 with a tailored pore size, Journal of Materials Chemistry 12 (2002) 3016-3020.

[23] H. Zou, S. Wu, Q. Ran, J. Shen, A Simple and Low-Cost Method for the Preparation of Monodisperse Hollow Silica Spheres, The Journal of Physical Chemistry C 112 (31) (2008) 11623-11629.

[24] J.Y. Ying, C.P. Mehnert, M.S. Wong, Synthesis and Applications of Supramolecular-Templated Mesoporous Materials, Angew. Chem. Int. Ed. 38 (1999) 56-77.

[25] H. Zhu, Z. Liu, Y. Wang, D. Kong, X. Yuan, Z. Xie, Nanosized CaCO3 as Hard Template for Creation of Intracrystal Pores within Silicalite-1 Crystal, Chem. Mater. 20 (3) (2008) 1134-1139.

[26] N. Yamasaki, T. Weiping, K. Jiajun, Low-temperature sintering of calcium carbonate by hydrothermal hot-pressing technique, Journal of Materials Science Letters 11 (1992) 934-936.

CHAPTER 5
Supporting Information

Simple Template-Technique for the Formation of Hollow Nano-sized Calcium Silicate hydrate Particles by Hydrothermal Approached

RESULTS:

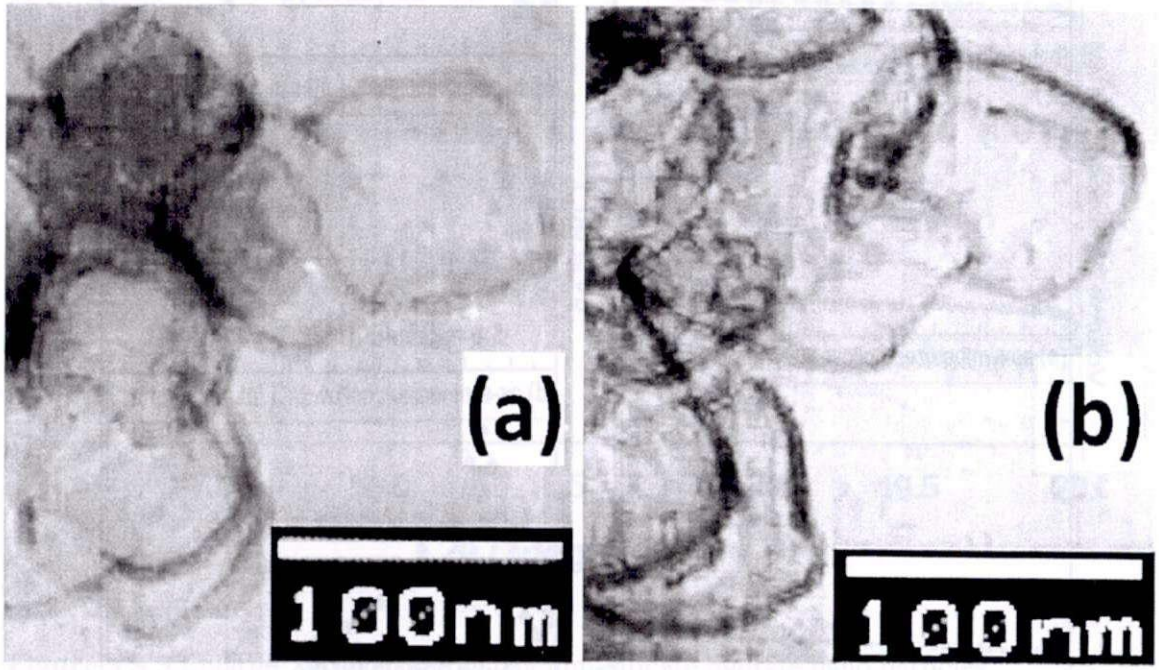

Figure 5.S 1 TEM images: Acid treated samples (a) [HS0dAH0ac] nano-sized hollow SiO_2 without hydrothermal, (b) [CS10d120H2ac] nano-sized hollow $Ca(OH)_2$-SiO_2 with hydrothermal at 120 °C for 10 d.

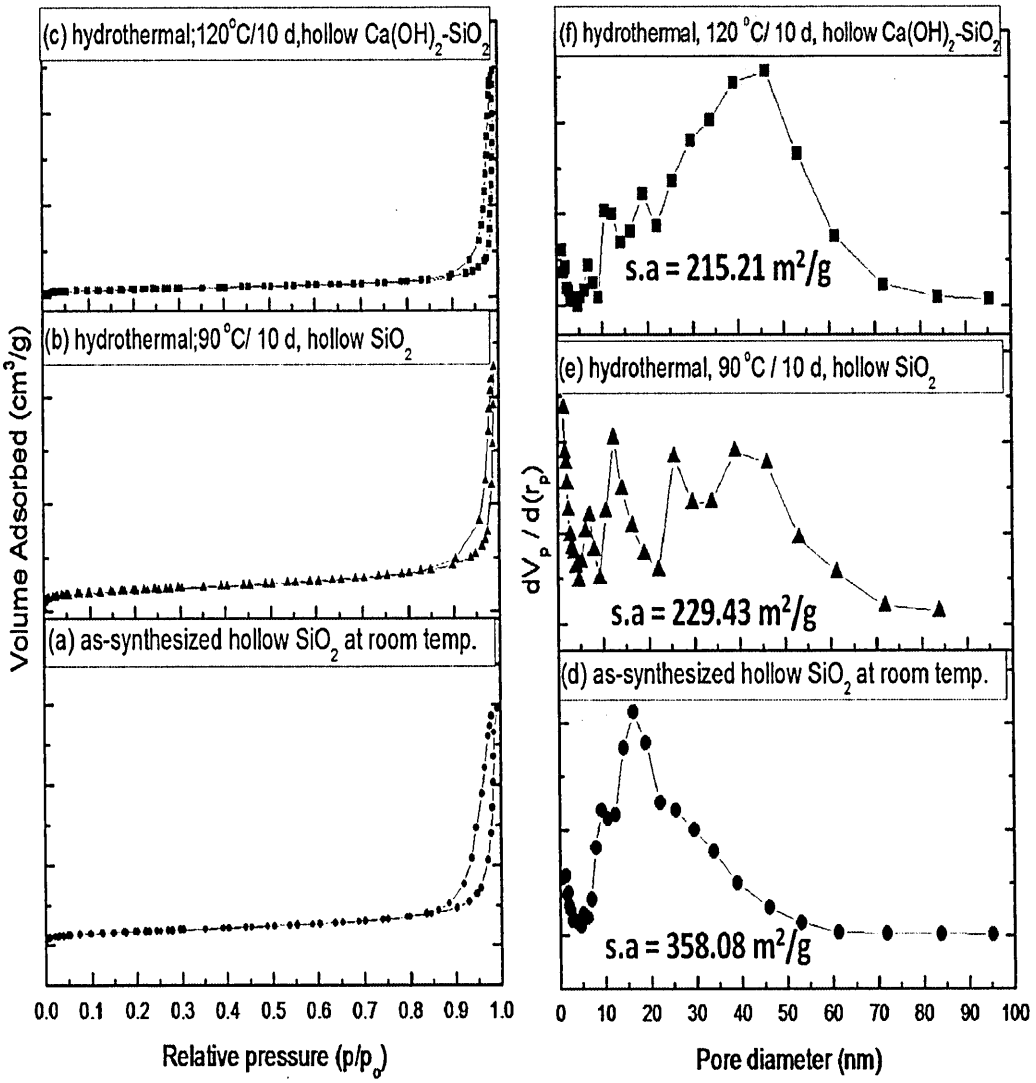

Figure 5.S 2 Nitrogen adsorption-desorption isotherms (a to c) and BJH differential pore size distribution (d to f) of hollow particles synthesized at ambient temperature (HS0dAH0ac), hollow particles hydrothermally treated at 90 °C for 10 d (HS10d90H1ac) and hollow calcium-silicate hydrate nanoparticles hydrothermally treated at 120 °C for 10 d (CS10d120H2ac).

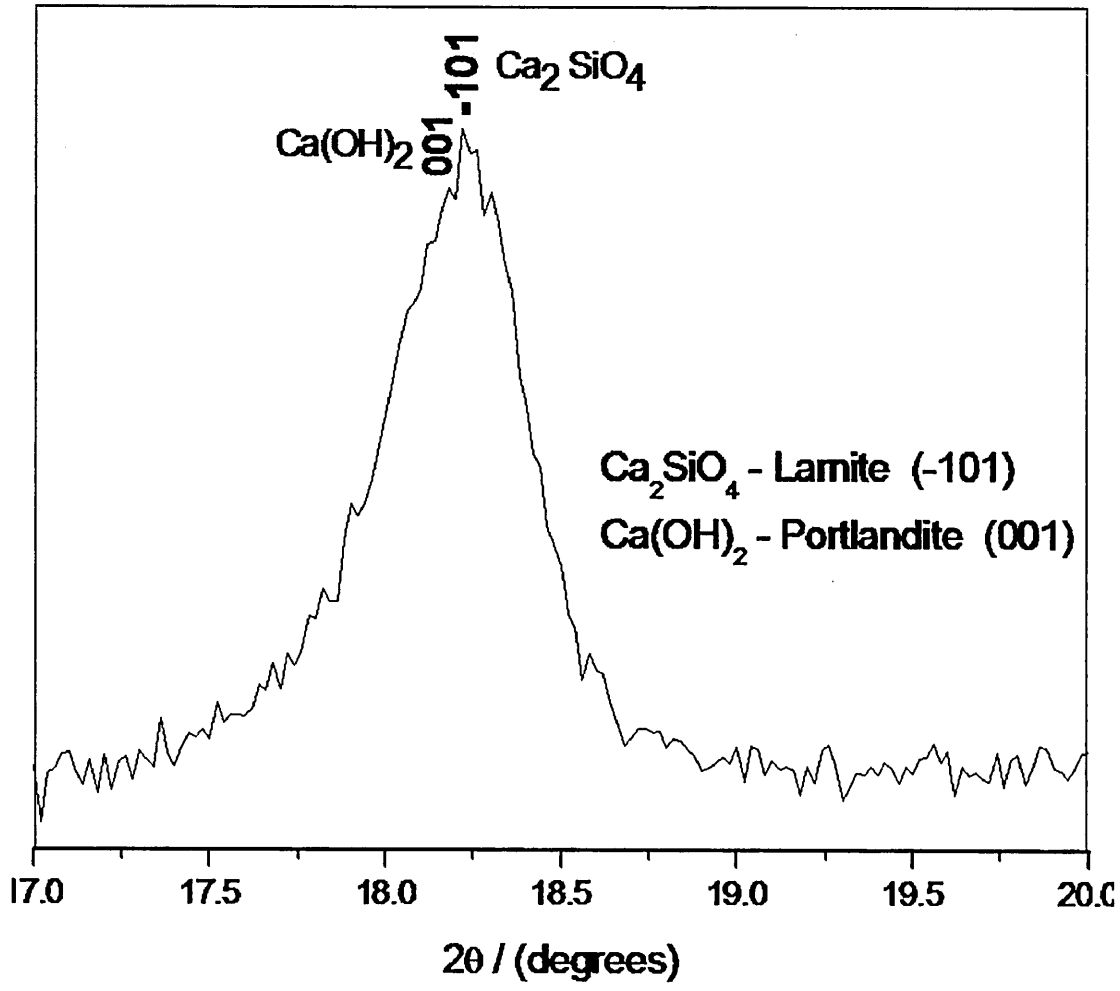

Figure 5.S 3 Enlarge XRD of hollow calcium-silicate hydrate nano particles hydrothermally treated at 120 °C for 10 d (CS10d120H2ac) ranging from (17.0 to 20.0) 2θ.

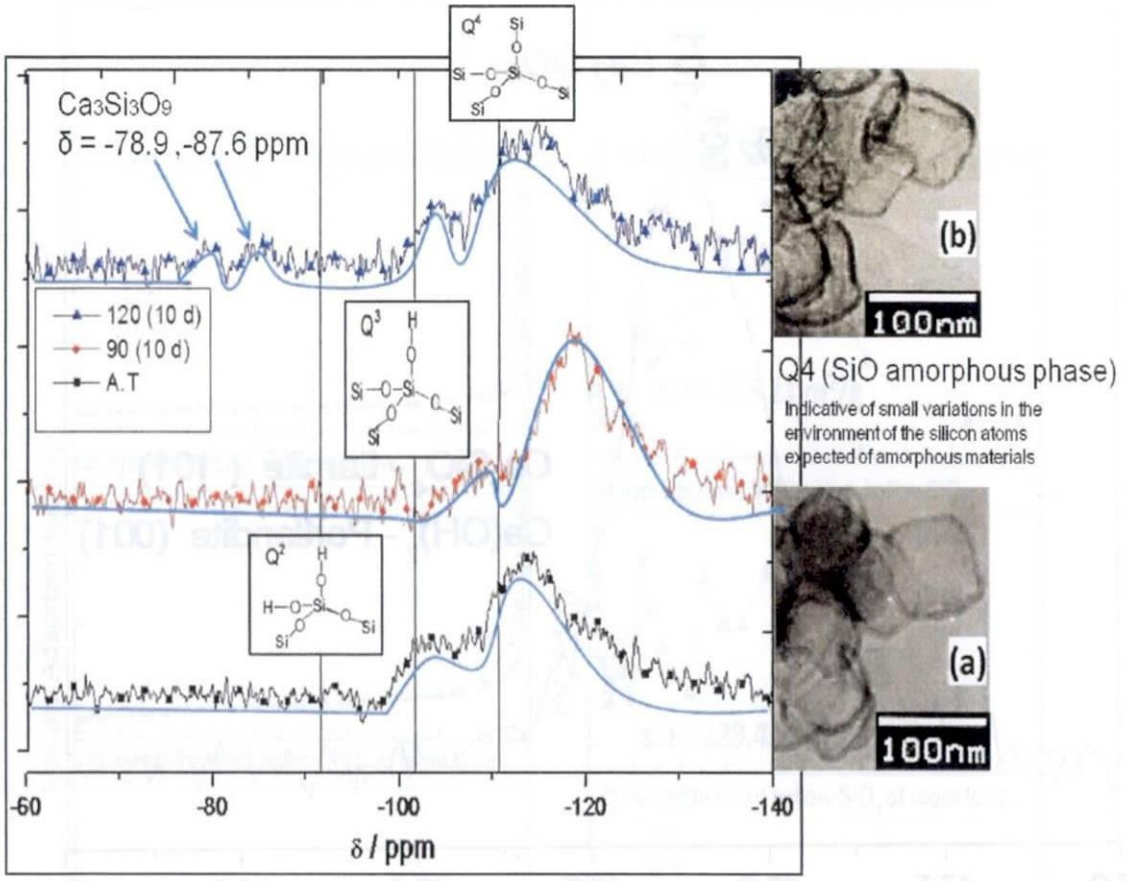

Figure 5.S 4 ^{29}Si NMR spectra. The C-S-H peaks have chemical shifts approximately -78.9 ppm and -87.6 ppm.[19]

CHAPTER 6

CONCLUDING REMARKS AND POTENTIAL DIRECTION FOR FUTURE RESEARCH

CHAPTER 6

CONCLUDING REMARKS AND POTENTIAL DIRECTION FOR FUTURE RESEARCH

6.1 Concluding remarks

This dissertation successfully characterized and fabricated nano- size and micro-size porous hollow silicate particles by template and double emulsion method. The investigated parameters were mainly on TEOS and NH_4OH concentration for template approach. While in fabrication of meso/macroporous shell hollow particles, surfactant CTAB for nano-size hollow SiO_2 with mesoporous shell and in double emulsion method, organic-water soluble Na-PA for microsphere hollow SiO_2 with macroporous shell were varied to optimized the pore distribution. Most of the syntheses were done at room temperature reaction except during the fabrication of hollow silicate with mesoporous shell wherein the temperature of the reaction and fabrication of hollow calcium-silicate hydrate nanoparticles was varied. The summary and conclusion of this thesis work are itemized as the following:

In chapter 2, a simple route in synthesizing nano- and micro-size hollow silicate particles with tunable shell thickness and unique anisotropic hollow shape by employing inorganic particles as template in conjunction with the sol gel method was fabricated. Calcium rich-Hydroxyapatite (CaHAp) nanoparticles (for nano-size hollow) and calcium carbonate ($CaCO_3$) micro particles (for micro-size hollow) in fabricating hollow silicate particles were used as inorganic core templates. The hollow silicate particles showed relatively stable anisotropic hollow shape with uniform shell wall thickness of silicate layers. In addition, the shell thickness and surface roughness have

tendency to increase with the increase concentration of tetraethyl orthosilicate (TEOS) precursor in ethanol solution. As expected, unique anisotropic shape and size of the hollow silicate particles depends on the inorganic template used.

In chapter 3, hollow silicate particles with micro, meso and macroporous amorphous silicate shell wall were fabricated. In this chapter, two processes were used such as double template method for nano-size hollow silicate particles with micro/mesoporous shell wall (NSHPMSs) and double emulsion method for micro-size hollow silicate particles with meso/macroporous shell wall (PHSM). For NSHPMSs, $CaCO_3$ (nano-size:60 nm) were used as core-template and cetyltrimethylammonium bromide (CTAB) for silicate network template. Then, by controlling the parameter such as CTAB, TEOS concentration and temperature reaction a hollow silicate nanoparticles with wormhole pattern micro/mesoporous shell were successfully generated.

While for PHSM, sodium polymethacrylate (water soluble polymer; Na-PA) was added into the aqueous solution of $water_1/oil/water_2$ (w_1ow_2) emulsion system with controlled parameters (emulsification rotational speed constant, fixed volume ratio and fixed surfactant ratio), modified (set-up) pressurized N_2 filtration and calcinations. Then, controlled hollow silicate microspheres with meso/macroporous shell were successfully prepared

In chapter 4, the precipitate sample for the adsorption of cationic (CTAB, cethyltrimethylammonium bromide) from aqueous solution onto nano-cube $CaCO_3$ particles under alkaline condition was schematically illustrated based on the obtained results and previous conducted data`s. A series of batch experiment were performed to determine the sorption graph of CTAB to nano-cube $CaCO_3$ particles. The experimental

studies were analyzed by TG-DTA weight loss (200°C to 400°C). The experimental data coincide to the reference model of typical adsorption isotherm of surfactant on solid oxide surfaces.

In chapter 5, fabrication/formation of stable hollow calcium-silicate hydrate nanoparticles by template ammonia-hydrothermal approached using $CaCO_3$ nano-size particles as core-template was successfully prepared. This simple process for the formation of a unique hollow calcium silicate (< 100 nm) nano-size particles, which was successfully set via the hydrolysis and condensation of tetraethylorthosilicate (TEOS), ammonia water (NH_4OH) and inorganic calcium silicate ($CaCO_3$) as template and then ammonia-hydrothermally treated. Then by varying the reaction ammonia-hydrothermal temperature reaction accompanied by variation of aging time, the formation of hollow calcium-silicate hydrate nanoparticles was understood. This approached for the formation of new nano-size hollow calcium-silicates hydrates particles can be a good alternative for the application on nano-bioactive materials.

6.2 Advantages and disadvantages of these approaches.

Evidently, advantage in template with (solid) $CaCO_3$ particles is possibly the most green approach, clearly effective, and most facile/common method for synthesizing hollow micro-/nanostructure. Aside from that $CaCO_3$ particles are technically abundant in nature and low cost material, they generally require no or minimal addition of surface functionalization and shell formation is guaranteed by chemical reactions. However the general disadvantages on this approach rely on achieving high product yields from this simple synthetics process, difficulty in forming a uniform coating around surfaces with large variation of curvature and lack of

structural robustness of the shells upon template removal. But these difficulties can be partly overcome by monitoring the acid concentration during acid etching, used of surfactant and exposed the core-shell particles thru hydrothermal approach for structural stability.

While for double emulsion approach (w_1ow_2) for fabricating macroporous hollow microspheres (PHSM), a key advantage of using double emulsion method for the preparation of PHSM is that the core removal stage is very easly eliminated. The liquid template, liquid cores (w_1) can be easily removed by low-stress generating processes such as evaporation, filtration or dissolutions with common solvent such as ethanol/water after the shell formation, final hollow product cannot be altered even it was calcined and has low parental toxicity because of the water –soluble polymer is used. However, the relatively low stability and the polydispersity of double emulsion approach may limit their application. Mostly controlling the microspheres, uniformity, and macroporous distribution into the shell still remain challenge. Moreover, the water-soluble polymer cannot be easily removed into the shell and liquid removal (w_1) is an energy-intensive process. But this problems can be partly overcome by calcination, pressure-filtration and controlling/monitoring the emulsion speed rate.

Finally based on the above findings, it is concluded that an eco-friendly approached in fabricating of nano-size and micro-size hollow silicate particles can be done. In general, by controlling the parameters enhance the surface morphology, porosity of the shell and stability of the hollow particles. The insights obtained from this non-toxic alternative mechanism will allow other researcher to gain better controls of the hollow particles especially in exploring the dispersion of the hollow particles. The

technique presented in this study provides a good foundation for the various future applications of the hollow silicate particles especially for template and double emulsion approached.

6.3 Potential directions for future research

The attainment in fabricating/synthesizing nano/micro-size hollow silicates particles have provided opportunities to tune their mechanical, optical, electrical, thermal, chemical and other properties. These advantages have in turn catalyzed exploration in a growing list of applications. However it should be noted that high-quality (e.g non-agglomeration) hollow silicates particles will be required in most cases for both fundamental research and practical applications. Based from the reported works, methods for producing high quality hollow silicates particles especially in non-toxic approach are still limited. Scaling-up these syntheses to produce commercial-scale quantities for applications is expected to introduce significant challenges for size, shape and shell thickness control.

In the present study, template and double emulsion approach is used to produced the nano-./micro-size hollow silicates particles. Further research should be conducted especially exploring organic-inorganic hybrid materials and with other metal alkoxides (such as titanium isopropoxide, aluminium isopropoxide, and others) especially for template approach in synthesizing nano and micro-size hollow particles. While for double emulsion methods, using different kind of water soluble polymers such as poly(sodium anetole sulfonate), poly(sodium vinylsulfonate) and poly(sodium 4-styrene sulfonate) for this approach should be explored particularly in controlling the macroporous shell of the hollow microspheres..

Extensive studies should be conducted on various kinds of organic-surfactants for fabricating hollow silicate nanoparticles with mesoporous shell walls (NSHPMSs). This is because, amongst these carriers made of silica, NSHPMSs stands out as a class of nonmaterial's with many distinctive advantages, such as having a non-toxic nature, good surface permeability, large specific surface area, tunable pore structures, excellent physicochemical stability and chemically modifiable surfaces. Particularly, potential hosts for various chemical agents/therapeutic drugs. NSHPMSs are especially useful when used to host therapeutic compounds such as enzymes that are easily degraded in the hostile biological environment when delivered per se without encapsulation. Besides encapsulation, these therapeutic agents can also be covalently attached, or adsorbed onto such silica nanocarriers that have been pre-surface modified. Thus, wide application of HMSNs has been in the field of biomedicine that includes its use as novel materials in catalysis, separation, cell-labeling and capsule agent for drug delivery.

Further detail investigation should be done on the formation of composite hollow calcium-silicate hydrates nanoparticles by ammonia-hydrothermal approach especially on the actual evidence of the attachment of calcia to silicate networks.

Hence, the improvement of the micro/nano-size hollow silicates particles will continue focusing especially on the eco-friendly preparation of controllable particles size and shell thickness. Technically, pore-size and nano/microstructure of the phase-shell are significant when permeability of hollow particles is considered in their applications. Additionally, simple approach to prepare hollow silicates particles with greater output and low cost production are genuinely expected especially for manufacturing production. In the applications of hollow silicate particles, it is important

to functionalize the interior of the hollow silicates to achieve preferred properties. Moreover the applications of hollow silicate particles in coating, thermal insulations, electronics and biological (bio-silicates) areas are promising and expecting future applications. This aspects of hollow micro/nano hollow silicates structures, offers exciting opportunities for newcomers to the fields.

LIST OF PUBLICATIONS,

CONFERENCES and

PROCEEDINGS

LIST OF PUBLICATIONS

CHAPTER 2

1. **Direct Template Approach for the Formation of (Anisotropic Shape) Hollow Silicate Micro particles**

   Raymond V.Rivera Virtudazo, Hideo Watanabe, Takashi Shirai, Masayoshi Fuji and Minoru Takahashi

   IOP Conference Series: Materials Science and Engineering 18 (2011) 062014

2. **Facile Preparation in Synthesizing Nano-size Hollow Silicate Particles by encapsulating Colloidal-Hydroxyapatite nanoparticles**

   Raymond V.Rivera Virtudazo, Hidekazu Tanaka, Hideo Watanabe, Masayoshi Fuji Takashi Shirai.

   Journal of Materials Chemistry 21 (2011) 18205

   NOTE: **APPLIED FOR PATENT**

CHAPTER 3

3. **Fabrication of calcined hierarchical porous hollow silicate micro-size spheres via double emulsion process**

   Raymond V.Rivera Virtudazo, Masayoshi Fuji, Takashi Shirai

   Materials Letters 65 (2011) 3112-3115.

4. **Simple Template Approach: Room-Temperature Synthesis of Non-spherical Nano-sized Hollow Silicate with Micro/Mesoporous shell structure.**

   Raymond V.Rivera Virtudazo, Masayoshi Fuji Takashi Shirai.

   Submitted to: Journal of Materials Chemistry (communication) under review

   NOTE: **APPLIED FOR PATENT**

CHAPTER 4

5. **Characterization of the precipitate sample for the Cetyltrimethylammonium bromide adsorp onto the nano-cube $CaCO_3$ particles from aqueous-ammonia rich solution**

   Raymond V.Rivera Virtudazo, Masayoshi Fuji, Chika Takai, Takashi Shirai

   Submitted to: Journal of Nanoparticle Research (Article) under review

CHAPTER 5

6. **A Simple Approach to form Hydrothermally Stable Templated hollow Silica Nanoparticles**

   Raymond V.Rivera Virtudazo, Hideo Watanabe, Masayoshi Fuji and Minoru Takahashi

   Ceramic Transaction Volume 219 (2010), 91-97.

7. **Facile Template-Technique for the formation of Hollow Calcium-silicate hydrate Nano-size particles by Hydrothermal Approach**.

   Raymond V.Rivera Virtudazo, Masayoshi Fuji Takashi Shirai.

   For Submition to: Communication format

   NOTE: **APPLIED FOR PATENT**

CONFERENCE and PROCEEDINGS

2008

- 21st Fall Meeting of the Ceramic Society of Japan, September 17-19, Kitakyushu, Japan (participant)

2009

- 65th Annual Meeting , Japanese Society of Microscopist, May 27-29, 2009, Sendai, Japan (Award winner, Exchange Program for Young Asian Microscopist (co-author))

  Mesostructure of Biphenyl-functionalized Organosilica Materials

  Eduardo Magdaluyo, Jr.[1], **Raymond Rivera Virtudazo**[2], Leonard dela Cruz[3], Herman Mendoza[1], Emily Castriciones[3]

- 38th Summer Seminar of The Association Tokai Young Ceramist, July 9-10, 2009, Toba Mie, Japan

  Templated Hollow Silica nanoparticles: Formation of Hydrothermally Stable Core-shell Silica

  Raymond V.Rivera Virtudazo, Hideo Watanabe, Takashi Shirai, Masayoshi Fuji and Minoru Takahashi

- International Center for Materials Research Summer Workshop: Novel Superconductors, August 2-15, 2009, University of California, Santa Barbara, USA (Only 50 postgraduate student carefully selected to participate)

  Proposed Research project: **"TEMPLATED HOLLOW NANOPARTICLES: PROPOSED FABRICATION OF A NOVEL SUPERCONDUCTOR"**

- The Third International Conference on the Characterization and Control of Interfaces for high Quality Advanced materials And Joining Technology for New Metallic Glasses and Inorganic Materials (ICCC1 2009), September 6-9, 2009, Kurashiki, Japan

  A Simple Approach to form Hydrothermally Stable Templated hollow Silica Nanoparticles

  Raymond V.Rivera Virtudazo, Hideo Watanabe, Masayoshi Fuji and Minoru Takahashi

- 2nd Thailand –Japan international Academic Conference, TJIA2009, November 20, 2009, Kyoto, Japan

  Hollow Silica Nanoparticles: Simple Technique to Stabilize the Amorphous Silica Shell by Hydrothermal-Templated Process

  Raymond V.Rivera Virtudazo, Hideo Watanabe, Masayoshi Fuji and Minoru Takahashi

2010

- World Congress on Particle Technology (WCPT62010), April 26-19, 2010, Nuremberg, Germany

  Synthesis of Nano-sized Hollow Calcium Silicate Particles by Template method Assisted with Hydrothermal Treatment

  Raymond V.Rivera Virtudazo, Hideo Watanabe, Takashi Shirai, Masayoshi Fuji and Minoru Takahashi

- 3rd International Congress on Ceramics (ICC3), November 15-18, 2010, Osaka, Japan

  Direct Template Approach for the Formation of (Anisotropic Shape) Hollow Silicate Microparticles

  Raymond V.Rivera Virtudazo, Hideo Watanabe, Takashi Shirai, Masayoshi Fuji and Minoru Takahashi

2011

- 日本セラミックス協会 東海支部 第42回 東海若手セラミスト懇話会 2011年 夏期セミナー

  42th Summer Seminar of The Association Tokai Young Ceramist, June 30-July 1, 2011, Gamagouri, Aichi, Japan

  Fabrication of Hollow Silicate Microsphere Particles with Meso/Macroporous shell wall by Double emulsion method

  Raymond V.Rivera-Virtudazo, Masayoshi Fuji, Takashi Shirai

- 24th Fall Meeting of The Ceramic Society of Japan, September 7-9, 2011, Hokkaido, Japan

  Simple process for the formation of Nano-size hollow silicate particles using HAp nanoparticles

  Raymond V.Rivera-Virtudazo, Hidekazu Tanaka, Hideo Watanabe, Masayoshi Fuji[1], Takashi Shirai

- 平成 23 年度中部談話会　研究・技術交流会

  - 日本の粉体産業を支える研究・技術 -

  粒子表面特性制御による粉体プロセスの効率化に関するワークショップ

  2011 年度若手研究者討論会

  日時：2011 年 9 月 15 日（木）、9 月 16 日（金）

  場所：紅葉屋　愛知県知多郡美浜町大字野間字畑中 9 番地

  Preparation of Nano-ellipsoidal Hollow Silicate particles using HAp nanoparticles by Template Approached

  Raymond V.Rivera-Virtudazo, Hidekazu Tanaka, Hideo Watanabe, Masayoshi Fuji, Takashi Shirai

ACKNOWLEDGEMENTS

ACKNOWLEDGEMENTS

Although this dissertation paper is individual work, I could not have than this without the help, guidance, effort and supports of people surrounding this project. It is with a great deal of fulfillment that I thank those who have contributed in the completion of this dissertation. First, with my deep sense of kind appreciation and admiration, I want to thank my supervisor, Professor Masayoshi Fuji, who continues to put up with his constant encouragement, kind support, invaluable guidance, and moral support concerning all my complications apart from the studies during my stay in Japan. I would also wish to express my thanks to my doctoral committee members Professor Koji Takagi and Professor Shinobu Hashimoto who provided valuable insights and constructive comments on the earlier version of my work to make it more scientifically relevant.

I would like to express my deepest gratitude to Prof. Minoru Takahashi, President of Nagoya Institute of Technology, for his professional advices and unselfish support during the progress of my doctoral studies. Despite his busy administrative and academic works, he always gave good comments and responded with great compliments towards my experimental works especially during our end-report seminar presentation.

I would like also to thank Dr. Takashi Shirai, Dr. Chika Takai and Dr. Hideo Watanabe for their generous support with invaluable advice during my doctoral course. I too wish to convey my sincere thanks to Ms. Chisato Takahashi for her invaluable help for observing my hollow silicate particles in TEM during entire periods of my research.

I wish to thank all the post doctoral researchers of Ceramics Research Laboratory (CRL) for various logical discussions on my research works. I greatly appreciate Prof. Lianying Liu College of Materials Science and Engineering, Beijing University of Chemical Technology (BUCT), Beijing, China for in-puts in the characterization of silica dispersion.

I am grateful to Mr. Seiji Yamashita (Ph.D student, my tutor) for his patience, understanding and kind help in assisting/conducting/introducing SEM, XRD and TG-DTA instruments and extending helps on filling up several Japanese application documents with the assistant of Dr. Tomoaki Kato, Mr. Fumikazu Kawajiri and Mr. Takahiro Iida. Special thanks to Mr. Takuya Asai for his actual demonstration on adsorption/desorption method and in synthesizing hollow silicate particles that leads to the foundation of my current study. Furthermore, grateful acknowledgment to undergraduates, graduates and all my friends at Ceramic Research Laboratory (CRL) for their kind help during the course of my experiment and made my research so intellectually stimulating and enjoyable

Many thanks are also extended to the office secretaries of CRL, particularly Ms Haruna Shirai, Ms Sakiko Endo, Ms Tomomi Hakashi, Ms Araki Tadashi and Ms Hisako Kuroishi, for their fast execution and processing of my pertinent official documents.

I wish to thank Monbukagakusho scholarship and Research Assistantship offered in the Processing Group of CRL for providing me enough financial support of my research work. I am also thankful to Assoc. Professor Ruben Menchavez, Professor Ephraim Ibarra, Professor Herman Mendoza, Professor Emily Castriciones and Professor Samuel Franco, for the encouragement in taking-up further studies.

Last, but not least, I would like to thank Almighty GOD for giving me and our family a good health and blessings all the time. I am grateful to my extended family in Iligan especially Aunt Mayet, Manang Inday and my Parents for their encouragement and moral support. A special thank goes to my sister Yvonne for her everlasting supports/prayers.

I would like to dedicate this thesis to **my Mother**, **Father** and **my late Aunt Ann** (adopted mom).

Raymond V.Rivera Virtudazo, Cer.E